Engineering Fracture Mechanics 241 (2021) 107349

Contents lists available at ScienceDirect

Engineering Fracture Mechanics

journal homepage: www.elsevier.com/locate/engfracmech

Application of configurational mechanics to crack propagation in quasi-brittle materials

L. Crusat, I. Carol *, D. Garolera

ETSECCPB (School of Civil Engineering), UPC (Technical University of Catalonia), 08034 Barcelona, Spain

ARTICLE INFO

Keywords:
Configurational mechanics
Crack propagation
Non-pre-established crack paths
Nodes relocation
Finite Element Method

ABSTRACT

The paper describes a numerical approach to represent cracking along non-pre-established directions, in 2-D structures or domains of quasi-brittle materials such as concrete or rock. The approach is developed on the basis of the FEM with zero-thickness interface elements, combined with the principles of Configurational Mechanics. Interface elements are pre-inserted along all potential crack lines in the mesh, and are equipped with a plasticity-type fracture mechanics-based constitutive model that incorporates fracture energies in mode I and IIa as constitutive parameters. Once an interface element starts cracking, an iterative re-orientation process is triggered according to the direction of configurational forces. After that process has converged, the interface orientation becomes fixed and the surrounding nodes are relocated to preserve mesh quality. The overall procedure developed has the main advantages of a fixed mesh topology (constant number of nodes) and a crack re-orientation criterion based on the minimization of the overall structural energy, as implied by the definition of configurational forces. Various examples of application are presented in which cracks get re-oriented during calculations. The results show good agreement with the crack paths known by symmetry considerations or experimental results, thus illustrating the good performance of the approach proposed.

1. Introduction

Modeling of crack initiation and propagation is of paramount importance in several Engineering fields such as Structural, Geotechnical, Mechanical, and recently also Petroleum Engineering. In recent decades, abundant literature has been published on the subject and considerable progress has been made in the representation of cracking and fracture using the Finite Element Method (FEM). In spite of that, the accurate and realistic prediction of crack initiation, propagation, and especially, crack trajectories, still constitutes a major challenge [1–5].

Early FEM implementations for crack representation were traditionally classified into smeared and discrete approaches. Smeared crack approaches, originally attributed to Rashid [6] were based on the use of classical continuum elements with nodal displacements, and included any opening/sliding of the discontinuities in an averaged manner within the continuum deformations. The cracking laws were considered part of the continuum constitutive laws with softening; “fixed crack” and “rotating crack” models are early examples of that representation [7]. The smeared approach had the advantage of a fixed mesh; however, a number of mathematical problems were soon identified such as a pathological mesh dependency and lack of uniqueness of the solution, or difficulties of the standard continuum elements to represent localized opening/sliding not aligned with the element sides, leading to unrealistically “thick” and

* Corresponding author.
E-mail address: ignacio.carol@upc.edu (I. Carol).

https://doi.org/10.1016/j.engfracmech.2020.107349
Received 16 December 2019; Received in revised form 8 September 2020; Accepted 24 September 2020
Available online 17 November 2020

stiff crack bands. A number of regularization techniques were proposed as remedies, such as the crack band model, non-local continuum, Cosserat continuum, gradient plasticity, or gradient damage [8–14]. However, although some of these methods have been shown to accomplish their main purpose of regularization, in general require sufficiently dense meshes in the zones subject to damage and fracture, the location of which is not generally known a priori. In recent years the phase-field approach has emerged as a powerful alternative [15,16,1]; however, this technique also seems to require denser meshes in the fracture zones [4,17] of location not necessarily known a priori, which in a general loading situation may imply the use of remeshing procedures [17–19].

The discrete crack approach, on its side, often attributed to Ngo and Scordelis [20], represents cracks explicitly by duplicating nodes and leaving the crack faces as free boundaries or, later (and more conveniently in case of crack closure or friction/sliding) by inserting zero-thickness interface elements [7]. The cracking criterion may be based on the LEFM theory [e.g. 21] or, more generally, on a cohesive law such as the Fictitious Crack Model (FCM) [22] or on generalizations of it using the normal and shear stress tractions in the form of a constitutive law for the cohesive interface elements [e.g. 23,24,25,26]. The original discrete approaches were linked to LEFM and implied continuous re-meshing in order to be able to represent, at least approximately, the singular stress state at the crack tip [21, FRANC code]. Later, however, with the use of zero-thickness interface elements, the option was developed of pre-inserting interface elements along the expected crack path if that is known a priori [7], or otherwise along all potential crack trajectories [27–30]. This would provide certain freedom for the crack to propagate, but has two shortcomings: (1) the increase in the number of nodes due to the systematic pre-insertion of interface elements, and (2) the restrictions of potential crack trajectories to the original mesh lines. The first problem is addressed by some authors by starting with a classical continuum mesh, resolving the stress tractions transmitted across neighbor elements and inserting the interfaces only when those stress tractions exceed the strength [31]. However, this requires quadratic elements, stress tractions can only be estimated easily at the middle nodes of each mesh line, and implies topological changes during the analysis. The second problem can be mitigated by using a proper meshing strategy that would include the main potential crack paths in the mesh, something that may be easier in some cases (e.g. if there is a material microstructure with known weakness planes/lines), but not so trivial in the general case. Developing an efficient method for crack propagation with non-pre-established trajectory is one of the main motivations of the work described in the present paper.

In recent years, a variety of other methods not clearly included in the smeared or discrete crack approaches have been also proposed, such as meshless methods, EFEM, XFEM, etc. [32–40]. Most of them reproduce some of the shortcomings of the smeared approach, that is, either the kinematics of localized deformation is not explicitly considered and its representation via continuum deformations requires very fine meshes in the areas of interest, or it is considered only internally within each element, therefore requiring external artifacts such as “tracking algorithms”, understanding as such the procedures not based on fundamental mechanics principles, which are intended to make discontinuities compatible across elements. Perhaps the most salient exception to these objections is the eXtended Finite Element Method (XFEM) in which the continuum deformation field represented by standard displacement formulation of the FEM is enriched with additional nodal variables with the meaning of displacement jumps, which are then interpolated with a discontinuous shape function defined only for the elements crossed by the discontinuity. The method, originally proposed by Möes et al. [41] has the advantage of representing fractures without the need of modifying the underlying mesh topology. A restricted version of XFEM for geomechanical applications has been proposed with multiple interacting but a priori fixed discontinuities, as it would correspond to the most relevant fractures found in a geological domain [42], and some key aspects of interpolation functions have been discussed in [43]. XFEM has also been used to simulate crack propagation, see e.g. [44,36,45,46] although the crack tip representation adds complexity in terms of the enrichment functions which have to include a singularity and may require special integrations techniques for the elements involved [47,48]. In the case of multiple discontinuities, each one of them requires one set of enrichment variables for the elements crossed, plus one additional set of interaction variables per each pair of crossing discontinuities, in the elements crossed by more than one intersecting discontinuity. If n is the number of unknowns per regular node, this means n extra additional unknowns for nodes of elements crossed by one discontinuity, $3n$ extra for nodes of elements crossed by two intersecting discontinuities, etc. [49]. Additional difficulties come from the required intersections of the XFEM discontinuity surface with the underlying mesh and the subsequent element subdivision for integration. This intersection may produce small badly shaped sub-elements that have been related to significant oscillations in the results, and generally require mesh corrections to either move close nodes away from the discontinuity or move them on top of it [43]. All that requires considerable bookkeeping and makes XFEM not trivial to implement for the general case with multiple propagating and potentially intersecting cracks, which in general would imply continuous changes in the number of variables for each node and the subsequent information to store/update. These complexities and possible remedies have been reported in XFEM literature [50–52].

With the general objective of developing a 2D crack propagation approach with no preestablished trajectories, another essential ingredient is the criterion for crack propagation and, especially, for crack propagation direction. As already mentioned, most of the existing procedures rely on local criteria at the cracking point, such as direction perpendicular to the maximum tensile stress [53–56]. However, Fracture Mechanics (FM) principles imply that the energy dissipated at crack sites comes mainly from elastic energy released by stress unloading in the surrounding areas. One powerful way to introduce those concepts in standard FE analysis may be achieved by means of Configurational Mechanics (CM), which is concerned with the overall elastic energy changes due to changes in the material configuration (i.e. the original geometry of the structure/domain). Applied in the FEM context, configurational forces may be interpreted as vectors indicating the direction in which the coordinates of each node should be moved, in order to maximize or minimize the change of the overall elastic energy of the structure. These forces are defined as derivatives of the elastic energy with respect to the initial position of the node (“configuration”), and their calculation involves an integral over the elements of the so called Eshelby pseudo-stress or energy-momentum tensor [57]. The concept has obvious application for fracture propagation, since configurational forces at the crack tip will indicate the direction in which that point should be moved (i.e. in which the crack should propagate) to maximize the overall elastic energy release. This idea, which has already been proposed and, to some extent also

developed, in the literature [58–61,2,15,62], seems the ideal way to provide the necessary (but often missing) energetically consistent criterion for crack propagation direction.

Based on the above considerations, a new model for 2-D fracture analysis is proposed in which crack initiation and propagation, including propagation direction, are not necessarily pre-established. The model is developed on the basis on the existing approach of pre-inserting zero-thickness interface elements along the expected crack path, or if that path is not known, inserting interface elements along a sufficient number of possible alternative crack paths, so that the crack(s) will get initiated during the calculations depending on local stress and boundary conditions. Once a crack has started to open, a procedure based on the configurational forces is established so that the corresponding interface element may get re-oriented to approach the actual physical direction of the crack. In this way, mesh topology (including number of nodes) is not changed during the re-orientation process, yet crack trajectories will evolve so that global structural energy will be minimized.

The content of the paper is organized as follows: after this introduction, Section 2 discusses the basic concept of configurational forces and Section 3 their physical meaning in the context of fracture mechanics and FEM calculations with cracks represented via zero-thickness interface elements. Section 4 describes the numerical implementation of the method including the procedures for interface realignment, as well as other numerical procedures involved such as mesh relaxation, variable transport and a new iterative strategy based on constitutive dissipation. Section 5 includes various examples of application showing the good performance of the approach developed and, finally, Section 6 contains some concluding remarks.

2. Basic concepts of configurational mechanics and interpretation of configurational forces

In the context of a general, large-strain formulation of the FEM, global elastic energy is a function of original location **X** as well as final node position after deformation **X**, i.e. $\psi(\mathbf{X}, \mathbf{x})$, and configurational nodal forces are generally defined as the negative gradient of energy with respect to the original node locations (at constant **x**):

$$\widehat{\mathbf{f}} = -\left.\frac{\partial \psi}{\partial \mathbf{X}}\right|_{\mathbf{x}=\text{const.}} \tag{1}$$

Developing this equation within the standard framework of a displacement-based large strain formulation of the FEM [63,64], configurational nodal forces may be expressed as:

$$\widehat{\mathbf{f}} = \int_{\Omega} \widehat{\mathbf{B}}^{\mathrm{T}} \Sigma \mathrm{d}\Omega \tag{2}$$

where, $\widehat{\mathbf{B}}$ is the non-symmetric version of the traditional "**B**" matrix in the FEM [65], and **Σ** is the "configurational stress" provided by Eshelby's energy-momentum tensor [57]:

$$\Sigma = W\mathbf{I} - \mathbf{F}^{T}\mathbf{P} \tag{3}$$

In the above equation, W is the elastic energy per unit volume of the undeformed configuration, **F** the deformation gradient and **P** the first Piola-Kirchoff stress. A similar expression may be obtained in small strains

$$\widehat{\mathbf{f}} = \int_{\Omega} \widehat{\mathbf{B}}^{\mathrm{T}} \widehat{\boldsymbol{\sigma}} \mathrm{d}\Omega \tag{4}$$

where the small-strain configurational stress has the following expression [64],

$$\widehat{\sigma} = \mathrm{W}\mathbf{I} - \mathbf{F}^{T}\boldsymbol{\sigma} \tag{5}$$

where $\mathbf{F}^{T}$ in small strain theory $F_{ji} = \left(\frac{\partial u_j}{\partial X_i} + \delta_{ji}\right)$.

The method implemented basically consists of "moving" the nodes (changing their coordinates) by certain magnitude along the directions indicated by configurational forces and, once moved, reevaluate configurational forces and repeat the process iteratively until convergence. Node relocation is obviously subject to some restrictions, such as for instance boundary restrictions not to change the domain geometry, as explained in Section 4.

3. Configurational forces and zero-thickness interface elements

In the current implementation, cracks are represented via zero-thickness interface elements [66–68] that can be re-oriented along the most favorable directions for crack opening/extension.

These elements are equipped with an existing fracture-based elasto-plastic constitutive law originally conceived to describe cracking in quasi-brittle materials such as concrete, rock, ceramics, ice, bone tissue, etc. [24,25]. The constitutive law is briefly outlined in the following; a more detailed description may be found in [24,25]. The elastic part of the interface response is controlled by normal and tangential stiffness coefficients K_N, K_T. Plastic behavior is based on a hyperbolic cracking surface which depends on three basic parameters: tensile strength χ, cohesion c and internal friction angle φ (Fig. 1a), according to the following expression:

$$\mathrm{F}(\sigma_N, \sigma_T) = -(c - \sigma_N \tan\phi) + \sqrt{\left((\sigma_T)^2 + (c - \chi\tan\phi)^2\right)} \tag{6}$$

The cracking surface evolves with a single history variable defined as the work dissipated in fracture processes, W^{cr}. In tension, the increments of W^{cr} are assumed equal to the increments of plastic work, while in compression only to the increments of shear work excluding basic friction. The surface evolves from the initial configuration shown in Fig. 1a, to a hyperbola going through the origin (no tensile strength) when , $W^{cr} = G_f^I$, and then the apparent cohesion starts to decay to the limit configuration of a pair of straight frictional lines when W^{cr}=G_f^{IIa}. Model parameters G_f^I and G_f^{IIa}correspond to the classical fracture energy in mode I, and to a second asymptotic mode II, or mode IIa, shear fracture energy under high compression and no dilatancy allowed. A typical stress-opening curve obtained for uniaxial tension is shown in Fig. 1b. More details of the formulation, numerical implementation and further examples under mixed-mode loading, may be found in [24,25].

Note that in the FEM approach to fracture using interface elements pre-inserted along all potential cracks ("FEM+z" approach), the interface elastic stiffness may be generally interpreted not as a physical parameter but as a penalty coefficient necessary to obtain the stress tractions along the interface plane, and for this reason (and in order not to introduce unrealistic spurious deformability along all mesh lines), very high stiffness values are typically used. A very high stiffness value causes elastic energy stored in the interface elements to be negligible in comparison to the elastic energy stored in the continuum elements and also in comparison to the fracture energy consumption upon crack opening (e.g. shaded area in Fig. 1b, in comparison to total area under the curve, G_f^I). This fact is relevant to the calculation of configurational forces (gradient of elastic energy), because then those forces can be calculated on the basis of the elastic energy which is stored in the continuum elements only, W_{el}:

$$\mathrm{W_{el}} = \int_\Omega w \mathrm{d}\Omega, \quad \text{where} \quad w = \frac{1}{2}\boldsymbol{\sigma} : \boldsymbol{\varepsilon} \tag{7}$$

Another peculiarity of FEM+z meshes is that they contain many duplicated/multiple nodes at the same location, as shown symbolically in Fig. 2a (in which interfaces are represented with a certain thickness and nodes are not coincident for clarity, but typically thickness is zero and all nodes at the same location really overlap each other). The group of nodes at the same location may be called a "cluster". In the implementation developed, the configurational forces of all the nodes in a cluster are summed to obtain the net configurational force that indicates the direction in which the cluster should be moved to decrease global elastic energy. For simplicity, when solving the configurational problem, an equivalent cluster mesh is generated without multiple nodes (Fig. 2b). In this way, the net configurational force is calculated over clusters and also location rearrangement is determined for clusters and later this information is transported to the nodes.

The sum of the configurational forces of all nodes in a cluster, and the subsequent movement of the cluster as a single entity in the interface re-alignment process, may also be interpreted from the configurational mechanics viewpoint. In a linear equation system, summing the forces of two nodes is the conjugate operation to the assumption that the corresponding displacements have to take the same value, i.e. they are the same variable. In this case, all nodes in the cluster will be moved together, so their configurational kinematic variables (coordinate change) will be the same and therefore the corresponding conjugate forces have to be summed. Configurational forces of opposite nodes in an interface represent energy changes associated to node relocation in the surrounding continuum on each side of the interface. If considered separately, some of those force components correspond to nodal relocations incompatible with the physical nature of the interface, for instance the no-interpenetration condition. Summing the cluster

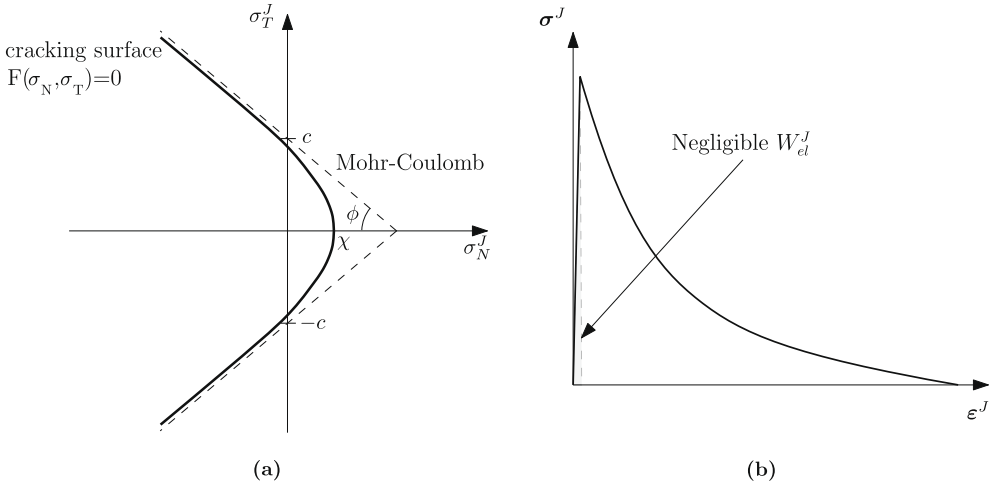

Fig. 1. (a) Hyperbolic cracking surface defined by three parameters. tensile strength χ, cohesion c and internal friction angle φ, which will evolve with energy dissipation; (b) resulting constitutive response in uniaxial tension, where the shaded area represents the elastic energy at peak (very small due to the high value of elastic stiffness).

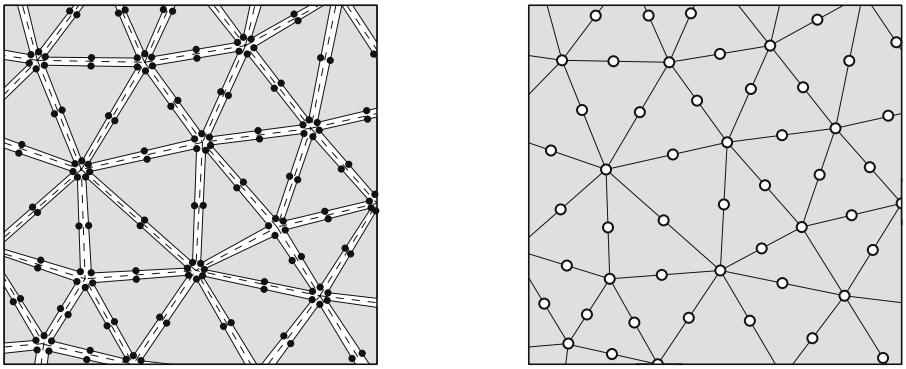

(a) (b)

Fig. 2. (a) Typical FEM+z mesh, where zero-thickness interface elements are represented with no-zero-thickness only for clarity and to be able to visualize individually the various nodes at each cluster. (b) Equivalent mesh without interface elements using clusters instead of traditional nodes.

components, those unphysical components cancel out, leading to a configurational force resultant on the cluster that could be interpreted as the directions in which the cluster as a whole should be moved, so that, after the resulting interface re-alignment, the energy release from the continuum surrounding the interface upon the same nodal displacement field (that is when that interface starts to open or slide), should be maximized.

4. Numerical implementation

As already mentioned, the main objective of the research described in this paper is to develop a method for crack realignment in the context of the general approach of FEM+z (FEM with zero-thickness interface elements pre-inserted in the mesh), in order to ultimately represent fracture development along non-pre-established paths in 2-D. It is well known that configurational forces are closely related to discretization error [63,64], and for this reason quadratic elements are going to be used in this implementation to reduce this error; however, element edges will be assumed straight to simplify the re-orientation process. Therefore, the initial mesh will include quadratic interface elements equipped with a fracture-based constitutive law, and in general their initial orientation will not correspond to the optimal/physical crack directions. As loading increases and one or more interface elements start to open (onset of cracking), an iterative re-orientation procedure will be initiated for those elements. This procedure conceptually constitutes an outer loop to the classical iterative loop for "deformational" analysis (material or geometrical non-linearity), i.e. only after the classical iterative process has converged, configurational forces are evaluated and the corresponding node locations may be changed. In general, the configurational forces obtained in this way may be non-zero for many nodes of the mesh. However, some of the mesh nodes should be considered as "configurationally prescribed" and not be relocated even if their configurational forces are non-zero, and for the remaining nodes a selective strategy for node re-location has been designed for computational efficiency, as explained below.

The first obvious set of nodes that should be configurationally prescribed is the boundary nodes, since the configurational forces for those nodes simply indicate the obvious fact that changing the domain shape/size might change the overall elastic energy (boundary nodes can in fact move along the boundary without modifying the domain; this partial restriction is considered later in the section). A second set of nodes that may be excluded from relocation (in spite of non-zero forces) is that of nodes not related to interfaces, or related to interfaces that remain closed. This is, in order to discriminate the energy changes, due to physical configurational changes (such as crack propagation) from those due to the "background noise" associated to discretization errors. A more detailed discussion on this particular aspect may be found in [63,64]. Finally, configurational changes are not permitted either for nodes that belong to interfaces that started cracking at earlier stages of the loading, and therefore their current location is already the result of some previous reorientation procedure. With all the above exclusions, the only nodes subject to potential relocation during configurational iterations are those corresponding to interface elements that have started cracking during the current load increment, and that do not belong at the same time to interfaces that were previously cracked.

On the other hand, practical implementation has shown that allowing a general reallocation of many nodes simultaneously may lead to lack of convergence of the configurational iterative process. This is why, in order to achieve a progressive configurational change, in the implementation developed it is not considered to relocate nodes that belong to more than one consecutive interface elements at the same time. Two interfaces are considered consecutive interfaces if they are connected to the same cluster (i.e. they may open one after the other in the context of a single propagating physical crack). In order to avoid that situation, if more than one consecutive interface would be starting to open during a given load increment, that load increment would be discarded, the load factor would be reduced and the calculation of the increment would be re-initiated. This process would be repeated until no more than one consecutive interface element would be opening during the same load increment (although more than one interface are allowed if they are not consecutive).

Note that, in general, progressive realignment of interface elements approaching the correct direction of physical cracks, may lead to crack initiation/propagation loads which might be lower for subsequent iterations until they become lowest when the orientation becomes optimal. Note also that the FEM+z analysis performed at each configurational iteration may exhibit snap-back depending on geometric configuration and parameter values. In order to cope efficiently with all those possible situations, an indirect displacement control (IDC) method may be required. This need, and the fact that the fracture-based interface element employed is governed by an energy-based history variable, has motivated the development of an IDC procedure based on energy dissipation, in which the external load factor is not fixed but is allowed to change during the iterative process. The detailed description of this IDC procedure may be found in [63,69].

During configurational changes the mesh may become distorted, or even entangled. This is why it may be convenient to limit the magnitude of the configurational changes for each iteration, and also to accompany the re-orientation process with some mesh improvement techniques. In the approach developed, a simple "mesh relaxation" algorithm capable of relocating the nodes around the interfaces just realigned, has been implemented. This procedure, which is explained below in more detail, is convenient to keep the mesh elements in regular shape and, in some cases, (such as the one presented in example 5.2, Fig. 21), to avoid mesh entanglement and element folding/overlap. Also, after changing nodal coordinates, it is necessary to map the values of displacements (and any other nodal variables), at the new node locations. This is the case for all the nodes which have been relocated, either due to configurational forces directly, or during the subsequent mesh-relaxation steps.

By definition, configurational forces $\widehat{\mathbf{f}}$ indicate the direction in which nodes should be moved so that the whole structure or domain experiences the fastest decrease in elastic energy. Therefore, the first and simplest "tangential approach" to modify nodal coordinates consists of moving the nodes of interest in the direction indicated by $\widehat{\mathbf{f}}$, i.e.:

$$\mathbf{X}_{new} = \mathbf{X}_{old} - \alpha\widehat{\mathbf{f}} \tag{8}$$

where α is a constant with a small value that is used to obtain the new nodal coordinates ($\mathbf{X}_{new}$) on the basis of the previous nodal coordinates ($\mathbf{X}_{old}$) and the configurational forces ($\widehat{\mathbf{f}}$). Some authors in the literature have used this technique in the context of mesh optimization in elasticity, on the basis of the idea that the optimal mesh geometry is the one that provides the lowest elastic energy [2,65,70].

This simple method, however, cannot be applied directly to the present case of fracture using FEM+z. Configurational forces based on elastic energy of the continuum elements will certainly indicate the direction in which crack should be extended to obtain the fastest decrease of elastic energy in the surrounding continuum; however, crack propagation will be subject to additional conditions such as the correct energy consumption per unit length (or area) of new crack that, according to Fracture Mechanics, needs to be dissipated. In this case, this should be guaranteed by the constitutive law of the zero-thickness interface elements, which incorporates this energy calibration via history variable W^{cr} and fracture energy parameters G_f^I and G_f^{IIa}. Note that only interface elements which are cracking for the first time are being re-oriented, and that, as it will be explained below, just after that the calculation of the latest relevant load increments is repeated with the new interface orientation. In this way, it is ensured that when the re-orientation process has converged the dissipation consumed due to fracture is the same as if the interface elements would have been correctly oriented from the beginning of the calculation, i.e. all the energy dissipated in the fracture process is accounted for by the underlying FEM+z analysis. According to those ideas, the three-step procedure described below and shown in Fig. 3 has been implemented. Note that this procedure only involves nodes connected to interface elements starting to crack in the current load increment, i.e. it does not include any node connected to interface elements already cracked in previous load steps:

1. The configurational force $\widehat{\mathbf{f}}^a$ at cluster "a" is projected on the direction normal to the initial interface element to obtain $\widehat{\mathbf{f}}_N^a$.

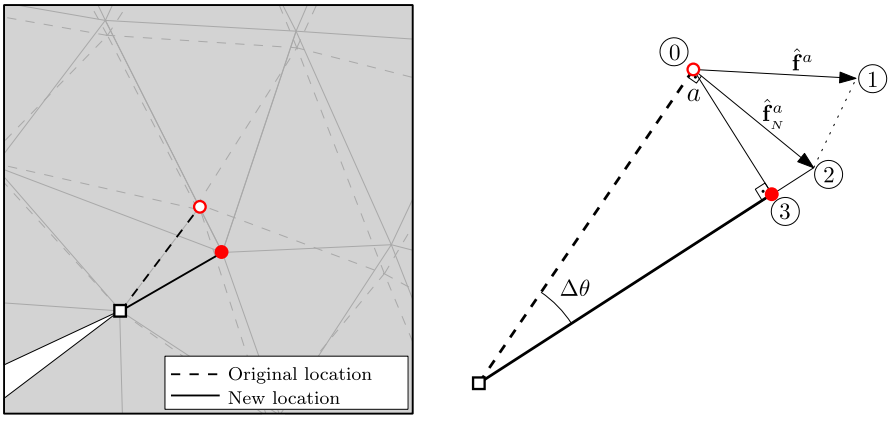

Fig. 3. Scheme of the procedure for nodal relocation of an interface element. Dashed lines represent initial mesh lines, and solid lines represent final mesh lines.

2. From this vector, only the fact that it points to the right or left of the original (dashed) interface line is retained, and the new interface line (solid) is then established by rotating the original interface line around its fixed end (point in which it connects to a previously open crack) by a given (small) angle $\Delta\theta$ in the direction indicated by $\widehat{\mathbf{f}}^a$ (in the current implementation $\Delta\theta = 1$ degrees). Note that, if the angle is small, this is equivalent to applying Eq.8 with $\widehat{\mathbf{f}} = \widehat{\mathbf{f}}_N^a$and the appropriate value of $c = c(\Delta\theta)$, which leads to a preliminary relocation of cluster "a" from original point "0" in Fig. 3, to point "2" in the same figure:

$$\mathbf{X}_{new} = \mathbf{X}_{old} - \widehat{\alpha}(\Delta\theta)\widehat{\mathbf{f}}_N^a \tag{9}$$

3. In order to reduce potential mesh distortion, the final interface element length is shortened slightly so that the final location of cluster "a" is point "3" in the figure (point from which the normal to the new direction leads to the original cluster location point "0").

Only for comparison, note that if Eq. (8) would have been applied directly with the original configurational forces $\widehat{\mathbf{f}}^a$ and a certain tentative (small) value of $\alpha = \widehat{\alpha}(\Delta\theta)$, the final location for cluster a would have been for instance point "1″ in the same Fig. 3.

It has been already mentioned that unless action is taken, the quality of the mesh may be degrading as the configurational process advances and the clusters progressively change their location. This is why a mesh relaxation strategy has been also implemented, which is performed after each step of the configurational process. Various techniques for mesh improvement with different degrees of sophistication exist in the literature, e.g. [71,72]. In this case, however, a simpler iterative strategy has been implemented to make mesh geometry more regular around each of the clusters moved during the configurational step and avoid ill-shaped continuum elements such as needle-type or "folded" elements during the crack reorientation (Fig. 4). The mesh relaxation procedure implemented is schematized in Algorithm 2, and summarized in the following: (a) a list is created with the clusters moved during the present configurational iteration or "configurational clusters"; (b) the clusters or nodes surrounding each of those are identified, in the current implementation this is done till the second layer (Fig. 5a); (c) for each of those clusters/nodes, the list of directly connected clusters/nodes is also identified, and its coordinates are set equal to the average of those connected clusters/nodes. Each of the clusters/nodes surrounding a "configurational cluster" are moved one after the other according to the procedure (c). The procedure is performed sequentially for each cluster of the configurational list, and then the whole process is repeated two or three times until no further changes are obtained in cluster locations, which leads to an improved mesh such as the one shown in Fig. 5b. Note that, as described, the above relaxation strategy is only applied to nodes/clusters which are configurationally free. This excludes the nodes/clusters located on the domain boundary and the nodes/clusters shared by interface elements that had already started cracking in previous configurational steps (Fig. 5a). The latter are considered totally fixed, but the former (boundary nodes/clusters) can be in fact allowed to move along the domain boundary. The practical benefits of this option is explored in example 5.2 in the following section.

Once the newly opening interfaces have been re-oriented and the surrounding mesh relaxed, the calculation needs to be restarted at a previous loading step. As previously explained, this is because, with a more favorable orientation, interfaces are likely to start opening at a lower external loading level, and therefore the last loading increment might need to be discarded. In the current implementation, the previous point in history to restart the calculation after each mesh re-orientation is the last previously converged configurational step, all the information of which needs to be properly stored in a configurational restart file.

However, before re-starting the calculation, the initial values of nodal variables for those nodes/clusters which have been moved, will need to be transported from their old to their new locations. Regarding Gauss point variables within elements, such as stress, strain or internal variables, in principle they would also need to be transported, although this is not necessary in case of linear elasticity since one can re-calculate strain from nodal displacements and subsequently also stress.

Fig. 6 illustrates the nodal transport process. The old mesh is represented in dashed lines, and the new one in solid lines. A node/

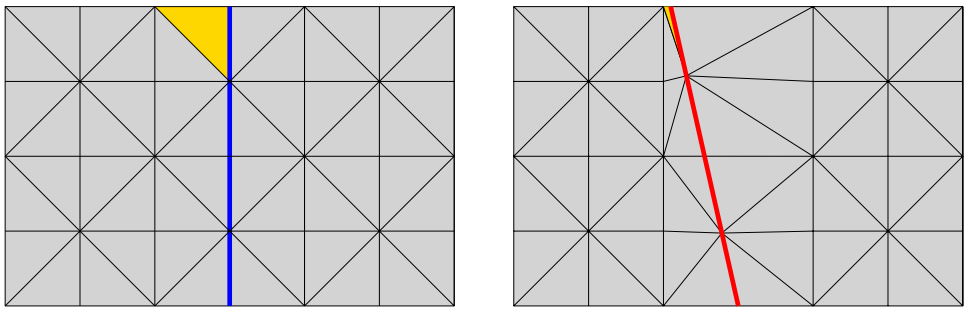

Fig. 4. Crack reorientation without mesh relaxation procedure. (a) original mesh configuration with initial crack path (in blue) and regular triangular continuum elements; (b) final mesh configuration after crack relocation (represented by red lines). The procedure of crack path realignment without an algorithm of mesh relaxation can cause ill-shaped elements such as the one colored in yellow. (For interpretation of the references to color in this figure legend, the reader is referred to the web version of this article.)

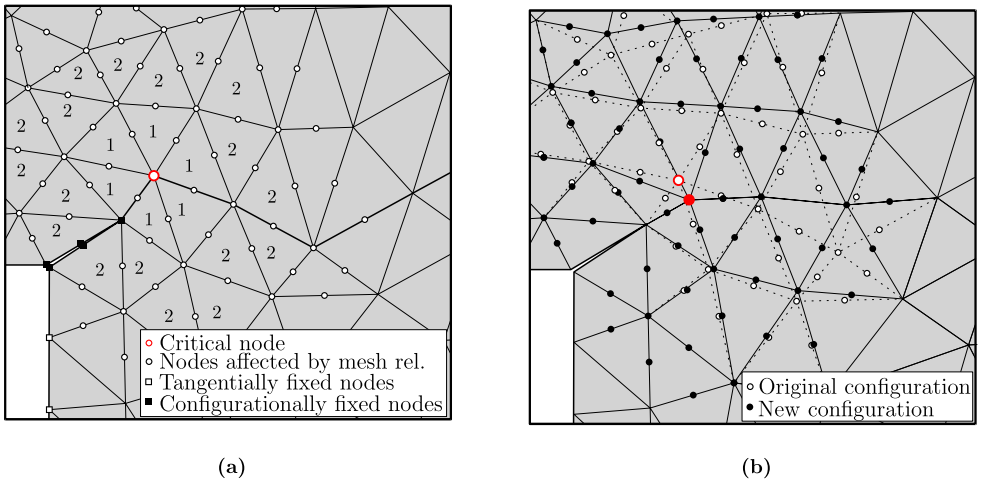

Fig. 5. Mesh relaxation procedure. (a) original mesh with cluster to be relocated during configurational iterations marked as a hollow red dot, and surrounding element layers "1″ and "2"; (b) final mesh configuration after configurational iterations and subsequent mesh-relaxation algorithm (original configuration represented by dotted lines). (For interpretation of the references to color in this figure legend, the reader is referred to the web version of this article.)

cluster represented with a hollow red dot in the old mesh, has been relocated to the solid red dot in the new mesh. The element in the old mesh which contains the new location of that cluster/node has to be identified and the local coordinates of that point need to be determined. Once this has been accomplished, it is immediate to interpolate nodal variables to the new locations with standard shape functions and nodal values corresponding to the old mesh configuration.

The overall scheme implemented for crack re-orientation based on FEM+z and configurational mechanics, is summarized in the Algorithm 1 scheme. Note that in this scheme, and for programming convenience reasons, the above-mentioned configurational outer loop has been merged with the load increment loop by use of some "goto" statements.

A final note is added concerning the possible extension of this procedure to three-dimensions. All fundamental concepts used in the approach and the algorithmic structure are equally valid in 3D, as well as most of the numerical procedures such as calculation of configurational forces, mesh relaxation, variable transport, etc. Only some specific geometrical concepts such as consecutive interfaces or procedures such as the node relocation strategy might require a new proper definition in the extended three-dimensional context.

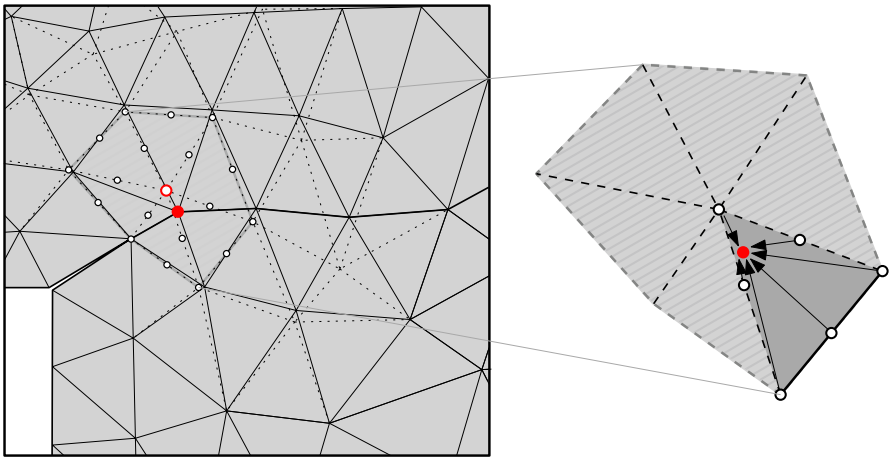

Fig. 6. Mapping of the nodal variables onto new location. (a) original mesh in dotted lines and final mesh in solid lines, and (b) detail of new node location (red point) on top of the old mesh for interpolation of transported variables. (For interpretation of the references to color in this figure legend, the reader is referred to the web version of this article.)

Algorithm 1. Configurational mechanics algorithm

Input: Model parameters, problem geometry and boundary conditions
Transformation of *"double/multiple nodes"* into *"clusters"*
Initialize deformational increment, *iincr* = 0
for *iincr* = 1, nincr *(Deformational Increment loop)* **do**
  Deformational increment convergence
  Evaluation of configurational forces
  Nodal configurational release (crack tip clusters)
  Create a list of the new cracked interfaces
  if consecutive interface elements have cracked[1] **then**
    Repeat last deformational increment reducing load factor
    goto *Deformational Increment loop*
  else
    for all selected free-clusters **do**
      if cluster not configurationally constrained **then**
        Change nodal coordinates:
          $X_{new} = X_{old} - \widehat{\alpha}(\Delta\theta)\widehat{\mathbf{f}}_N^a$
        List moved clusters
        if *Configurational convergence* reached **then**
          Fix moved clusters
          Mesh-relaxation + Mapping of nodal variables
          iincr = *iincr* + 1
          goto *Deformational Increment loop*
        else
          Release moved clusters
          Mesh-relaxation + Mapping of nodal variables
          Repeat deformational increment since *last*
          Configurationally converged Increment
          goto *Deformational Increment loop*
        end if
      end if
    end for
  end if
  iincr = *iincr* + 1
end for

[1]Previously two lists must be created: The list of consecutive interfaces (interfaces connected to the same cluster) and the list of cracked interfaces able to be moved in the current configurational step. Then, check that there are non-consecutive interface elements in the list of cracked interfaces able to be moved.

Algorithm 2. Mesh Relaxation Subroutine

Input: List of moved clusters, geometry connectivities
for *r* = 1,*nrepetitions* **do**
  for *i* = 1,*ncluster* **do**
    icluster = *clusterList*(*i*)
    CALL subroutine that identifies free clusters surrounding moved
  icluster (until second layer) to calculate the arithmetic mean of
  cluster coordinates:
    $\mathrm{x(icluster)} = \frac{\mathrm{x_1} + \mathrm{x_2} + \cdots \mathrm{x_n}}{\mathrm{n}}$
    Assign new coordinate (**x**) to the corresponding cluster/nodes
  end for
end for

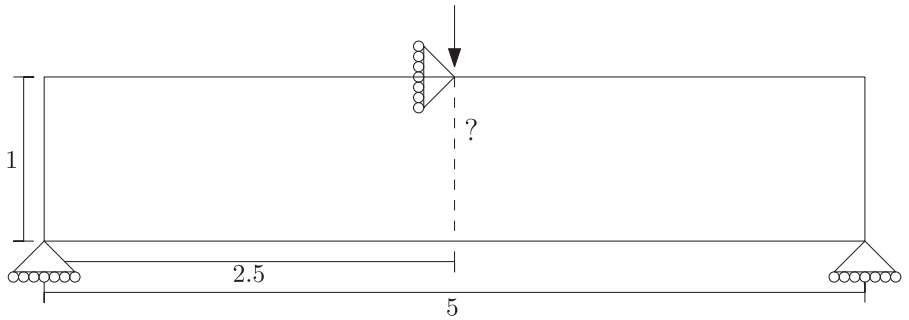

Fig. 7. Boundary conditions of three-point bending test example.

5. Examples

5.1. Three-point bending beam test with a single crack path

The first example of application to crack propagation is a 5 × 1 m three-point bending beam test represented in Fig. 7. It is a simple and useful example to verify simulations of cracking along non-pre-established path because, due to symmetry, it is known that the crack path should be vertical, along the plane of symmetry and starting from the bottom face of the beam. The initial mesh lines are generated randomly, and if the process works correctly, the initially zig-zagging mesh lines should get realigned to this vertical crack path.

Deformational boundary conditions consist of nodes at the lower vertices vertically constrained, and a node at the middle of the upper face with horizontal displacements restricted. The loading is applied as a vertical displacement at the prescribed point and it has an increasing value (Fig. 7).

The beam is discretized into triangular elements of quadratic order (Fig. 8). The configurational iterative procedure is adjusted so that the change of interface orientation at each iteration does not exceed 1°, and the iterative strategy for the deformational iterative procedure is the indirect displacement control based on fracture dissipation [69], with an automatic adjustment of the value of dissipation constraint during the deformational increments. Due to the expected crack trajectory, and in order to deal with increasing complexity more progressively, in this first example interface elements are pre-inserted along a single line zig-zagging around the symmetry line of the beam (blue line in Fig. 8).

The continuum material is linear elastic (small strain), with elastic modulus $E = 15000$ MPa and Poisson's ratio $\nu = 0.0$. The parameter values used for the fracture-based constitutive model are the following: normal and tangential elastic stiffness $K_N = K_T = 10^7$ MPa/m, friction angle $\tan\varphi = 0.7$, tensile strength $\chi = 3$ MPa, cohesion $c = 6$ MPa, fracture energy mode I $G_f^I = 10^{-2}$MPa·m, fracture energy mode IIa $G_f^{IIa} = 10^{-1}$ MPa·m and sigma at which dilatancy vanishes $\sigma_{dil} = 30$ MPa.

As expected, the crack is initiated at the center of the lower face of the beam and from there it propagates upwards. In Figs. 9 and 10 the final state of the beam is depicted, showing that the iterative configurational process succeeds in orienting the crack along the correct vertical direction. In the figures, blue lines correspond to the zero-thickness interface elements which remain un-cracked and, therefore, in the scheme implemented they have not triggered the process of moving nodes (although some of them may have changed orientation if they share nodes with other interfaces already cracked, such is the case of the top interface in Figs. 9 and 10). Red lines correspond to the interface elements that have started cracking, and therefore configurational forces may have moved them to an optimal position.

Fig. 11 depicts two load-displacement curves for the same beam, the first one in blue corresponds to a calculation with the initial mesh configuration fixed, which results in a distorted zig-zagging crack trajectory, and the other one in red has been obtained with the crack realignment strategy leading to the vertical straight crack path. As it could be expected, the load-displacement curve obtained in the second case exhibits a lower, more realistic peak and post-peak response. This is because in the final configuration interface elements are better oriented and therefore the crack initiates and propagates with lower applied load values.

5.2. Eccentric three-point beam bending test with one possible path

The second example consists of an eccentric three-point bending beam, where the initial notch is not aligned vertically with the loading point of prescribed displacement at the middle of the top side of the beam [73,74]. The desired path must follow some inclined line connecting the notch tip with the loading point, as depicted in Fig. 12.

The beam is discretized into triangular quadratic elements and the initial path trajectory is defined by twelve interface elements that zig-zag from the tip of the notch until the loading point at middle top of the beam (Fig. 13). Material properties for the continuum (assuming small strain and linear elasticity) are Young's modulus $E = 10000$ MPa and Poisson's ratio $\nu = 0.2$ and for the interfaces are: $K_N = K_T = 10^5$ MPa/m, $\tan\varphi = 0.7$, $\chi = 3$ MPa, $c = 9$ MPa, $\sigma_{dil} = 50$ MPa. For the fracture energies in mode I and IIa, in the first round of calculations some relatively high values have been assumed ($G_f^I = 10^2$ MPa·m, $G_f^{IIa} = 10^3$ MPa·m) in order to simulate perfect plasticity and facilitate convergence. The remaining options are similar to the previous example.

At the end of the calculation process, interface elements are reoriented replacing the unlikely zig-zag path to a smooth and slightly curved line trajectory, as seen in Figs. 14 and 15, where blue lines represent the interface elements still not cracked and red lines are the ones that have already cracked and therefore may have been moved to the optimal position by configurational forces.

Load-displacement curves of Fig. 16 show that solving the problem with the fixed geometry provided by the initial configuration

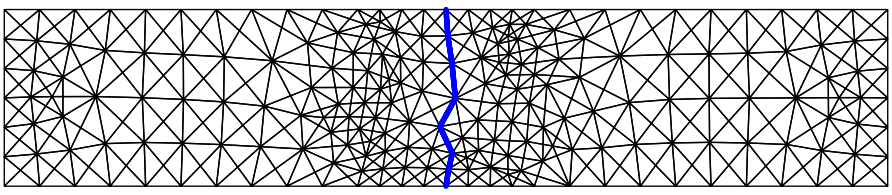

Fig. 8. Initial configuration of the mesh and interface elements.

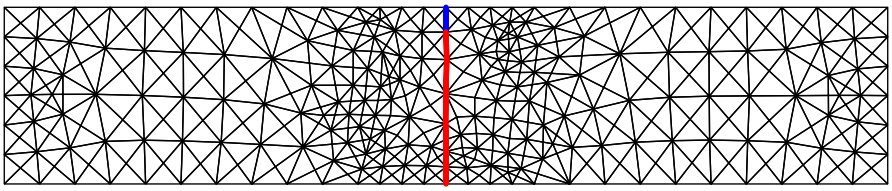

Fig. 9. Configuration with interface elements realigned at the end of analysis.

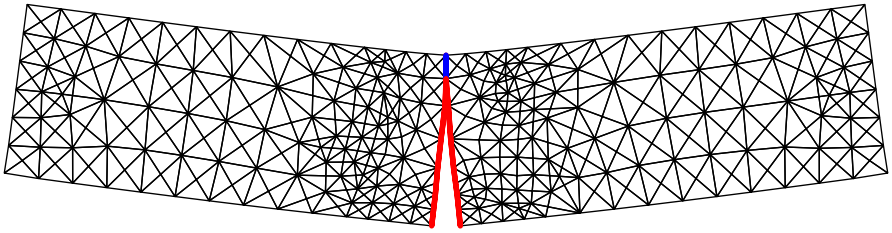

Fig. 10. Deformed mesh at the end of analysis (magnification ×100).

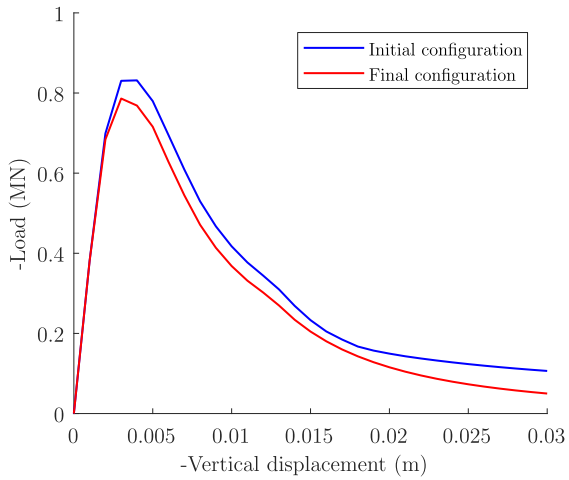

Fig. 11. Three-point bending test load-displacement curves.

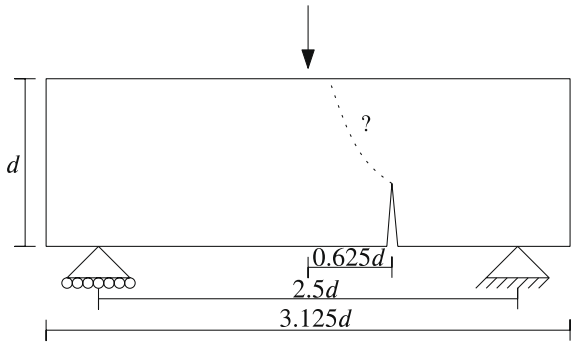

Fig. 12. Boundary conditions of eccentric three-point bending test example assuming $d = 1$ m.

leads to clearly higher loads than using the mesh with the interfaces realigned. In these calculations, load-displacement diagrams show always- hardening curves due to the assumption of very high fracture energy which is equivalent to near-perfectly plastic interface behavior.

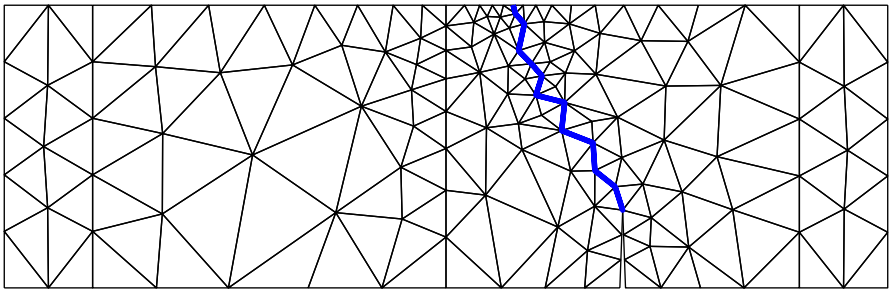

Fig. 13. Initial configuration of eccentric three-point bending test example.

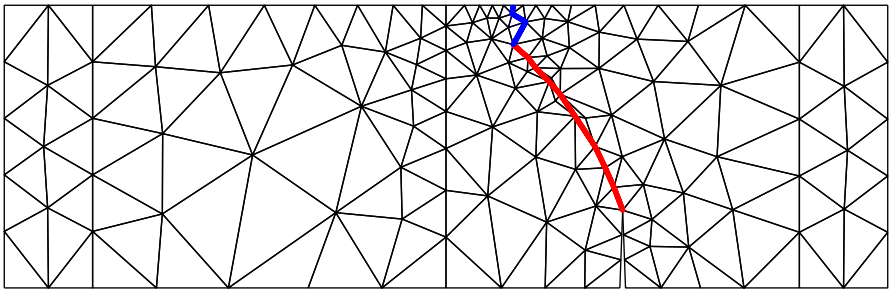

Fig. 14. Final configuration of mesh and interfaces for the eccentric three-point bending beam.

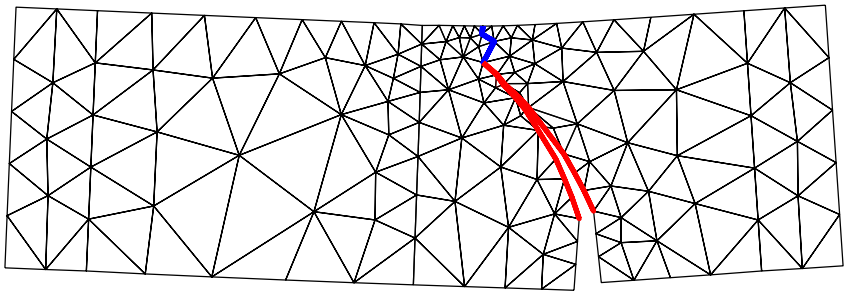

Fig. 15. Deformed mesh and interfaces for the eccentric three-point bending beam (magnification $\times 10$).

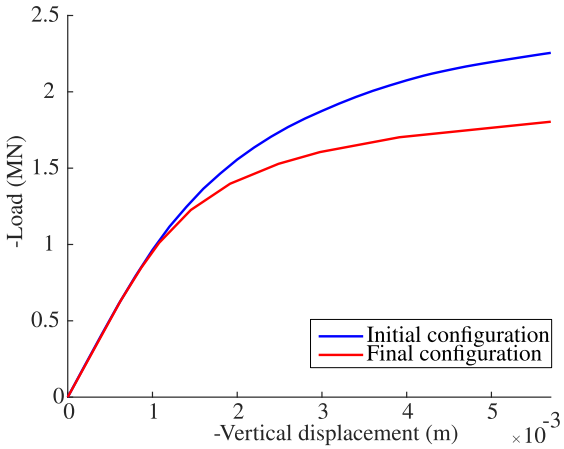

Fig. 16. Eccentric three-point bending test load-displacement curves obtained using a very large fracture energy value ($G_f^I = 100$MPa·m).

Additional calculations have been run with identical parameters except for the fracture energies, which take lower, more realistic values $G_f^I = 0.01$ MPa·m or $G_f^I = 0.001$ MPa·m and, in both cases. Results are depicted in Figs. 17–20. Figs. 17 and 18 show the final crack geometry and deformed shape of specimen for each value of G_f. These results seem similar to the case of perfect plasticity (Fig. 15). However, the crack paths are different, as it can be seen in Fig. 19, which shows that with perfect plasticity the crack trajectory near the tip follows a lower path, which turns out progressively higher for lower values of G_f. Therefore, an interesting observation is that by means of the present approach one can evaluate the non-trivial influence of material parameters on crack trajectory.

Fig. 20 shows the load-displacement curves corresponding to each value of G_f and the final crack geometry (in red), together with the curves that would have been obtained for each value of G_f by using the original crack geometry (no reorientation, in blue). Crack reorientation with the same G_f leads to lower peak load and lower peak deformations, which shows the benefit of the reorientation strategy implemented. On the other hand, the effects of changing G_f are also clear, with lower peaks and softening curves (more brittle) for lower G_f values, in contrast to the always increasing (hardening) curve obtained for perfect plasticity.

Finally, this example also shows that the mesh relaxation algorithm, which has been previously presented as a strategy to maintain the mesh quality (Section 4), in practical cases may be completely necessary to achieve the right representation of the crack path. As shown in Fig. 21, if only reorienting interface elements without the subsequent mesh relaxation process, reaching the crack final trajectory (in red) would imply element folding due to the superposition of lines.

This example of the eccentric three-point bending beam has been also selected to verify an extension of the mesh relaxation technique implemented, that consists of involving also the boundary nodes. As already explained, the boundary nodes have been considered configurationally fixed, as a sufficient condition to ensure that node relocation would not affect the domain geometry. However, strictly speaking the domain boundary could be equally preserved if those nodes (excluding domain corner nodes) would be allowed to move *along* the boundary. To explore this possibility, the extension has been tentatively implemented and tested in the case of this beam with the lower fracture energy value $G_f^I = 0.001$ MPa·m. As seen in Figs. 18 and 19, for this lower value of G_f^I the crack would tend to develop more vertically, and because the boundary node could not move the line of interfaces would be progressively stretched from the end of the open crack to this boundary point. As the result the configurational strategy could only proceed until the crack has reached a point at two segments distance from the upper face of specimen. As a first approach to explore the effects of moving nodes along the boundary, those nodes have been also included in the mesh relaxation procedure, and once their new location has been computed, they have been projected back onto the boundary. The results of applying this strategy in this example, are shown in Fig. 22. As seen in the figure, the movement of the boundary nodes along the domain boundary makes it possible the re-orientation and the crack progression by one extra interface element, therefore till a point only one short segment away of the upper beam boundary.

5.3. Two-notch beam

The third example consists of the two-notch mixed-mode fracture beam originally tested by Nooru-Mohamed and van Mier at TU-Delft [75], and also analyzed numerically in later studies [74] and [76]. The specific geometry and parameters used in the present analysis have been extracted from [76]. Geometry and boundary conditions are depicted in Fig. 23. This example has been chosen in order to verify the performance of the approach proposed in a case with simultaneous development of more than one non-consecutive cracks.

The beam is discretized with quadratic triangular continuum elements, and the mesh is a little finer in the zone of interest (central part of the beam between and around notches), see Fig. 24. From the experimental results of [76] it is known that for these conditions two cracks are formed that start at the tip of the notch and grow towards the load/displacement application points. Consequently, two zig-zagging lines of interface elements have been preinserted along mesh lines connecting the top and bottom notches on each side of the beam ligament. Initially irregular paths have been selected to simulate the crack propagation (blue lines in Fig. 24), that should be realigned during configurational iterations. The material model for the continuum is linear elasticity (small strain) with Young's modulus $E = 30000$ MPa and Poisson's ratio $\nu = 0.18$. The interface parameter values are: $K_N = K_T = 10^8$ MPa/m, $\tan\varphi = 0.7$, $\chi = 2.7$ MPa, $c = 15$ MPa, $\sigma_{dil} = 27$ MPa and fracture energy mode I and IIa, $G_f^I = 1.1 \cdot 10^{-4}$ MPa·m and $G_f^{IIa} = 1.1 \cdot 10^{-3}$ MPa·m.

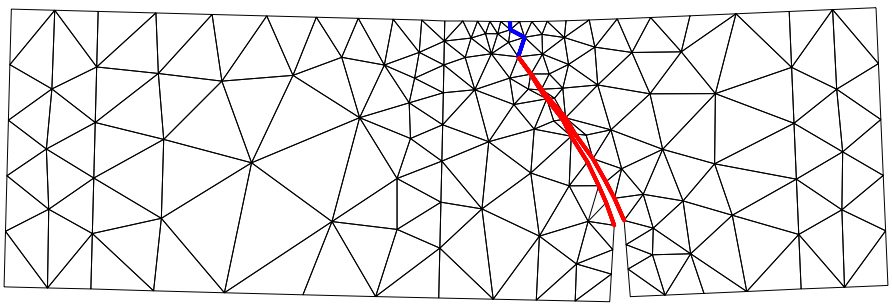

Fig. 17. Eccentric three-point bending test deformation with $G_f^I = 0.01$ MPa·m and $G_f^{IIa} = 10G_f^I$ (displacement magnification ×10). final mesh configuration and deformed shape.

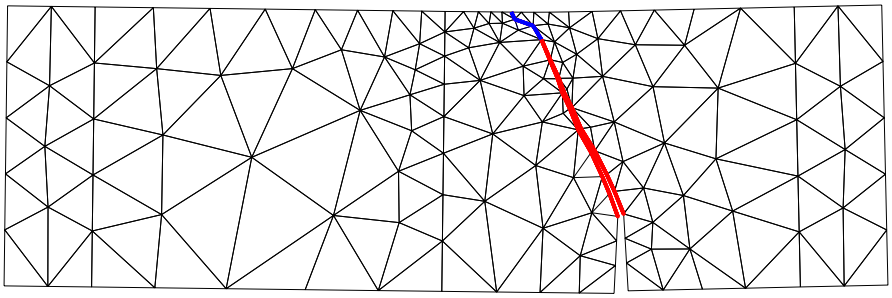

Fig. 18. Eccentric three-point bending test with $G_f^I = 0.001$ MPa·m and$G_f^{IIa} = 10G_f^I$ (displacement magnification $\times 10$)**.** final mesh configuration and deformed shape.

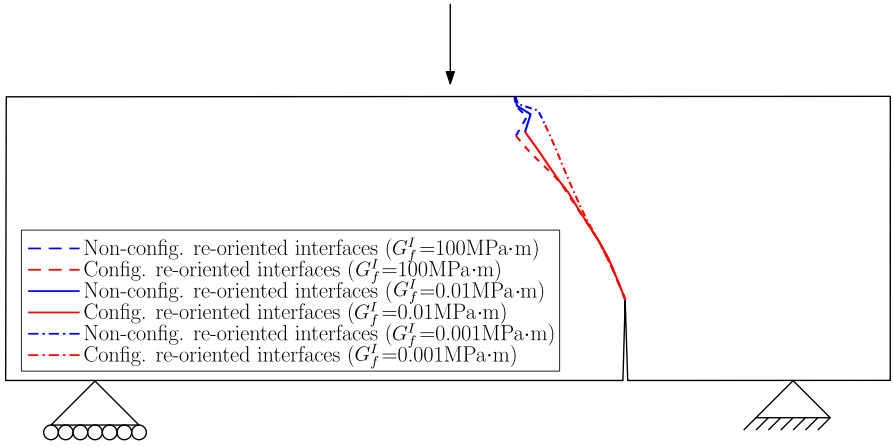

Fig. 19. Eccentric three-point bending beam test**.** Comparison of final crack orientation path depending on G_f values.

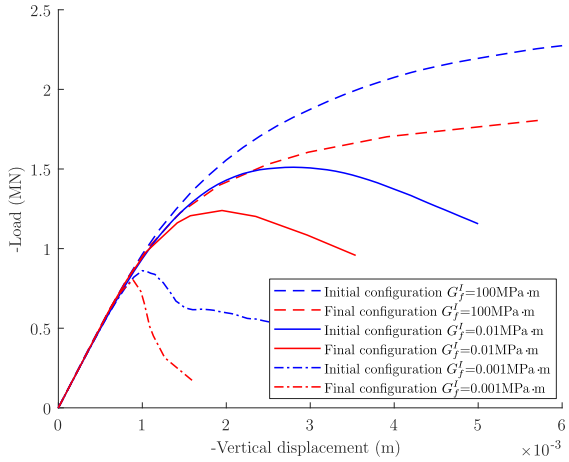

Fig. 20. Eccentric three-point bending test load-displacement curves depending on G_f values.

During the iterations of the deformational/configurational analysis, the interface orientations and locations are modified, and the resulting final deformed mesh is shown in Fig. 25 on the initial geometry, together with the area of cracking observed in experiments [76]. In Fig. 26, the same results are depicted on the deformed geometry. Same as in previous examples, the interface elements which have not reached cracking remain in blue color, while red lines correspond to those interface elements which have cracked. As shown in the figure, the cracked interfaces have been realigned nicely to configure a pair of smooth curved wing cracks which embrace a central bridge of solid material crossing the ligament from top left to bottom right, consistently with the kinematics of the prescribed displacements.

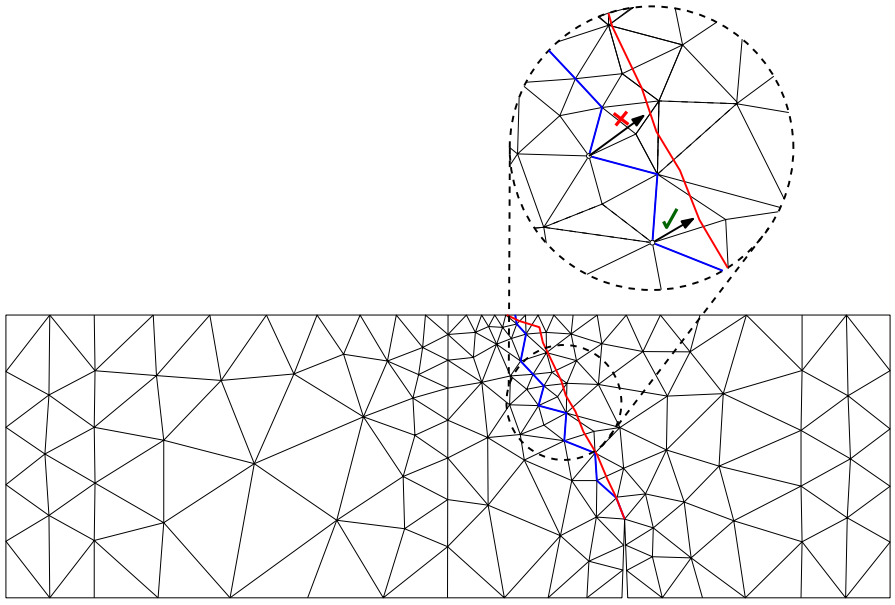

Fig. 21. Final crack path (in red) represented over the initial configuration of the eccentric three-point bending test example. Focusing on the enlarged view of the zone of interest, the arrows indicate the location change of selected end nodes of the interface elements. Note that some of them remain within the same continuum element but some others move to a different element, which, in the absence of mesh relaxation would imply element folding and mesh entanglement. (For interpretation of the references to color in this figure legend, the reader is referred to the web version of this article.)

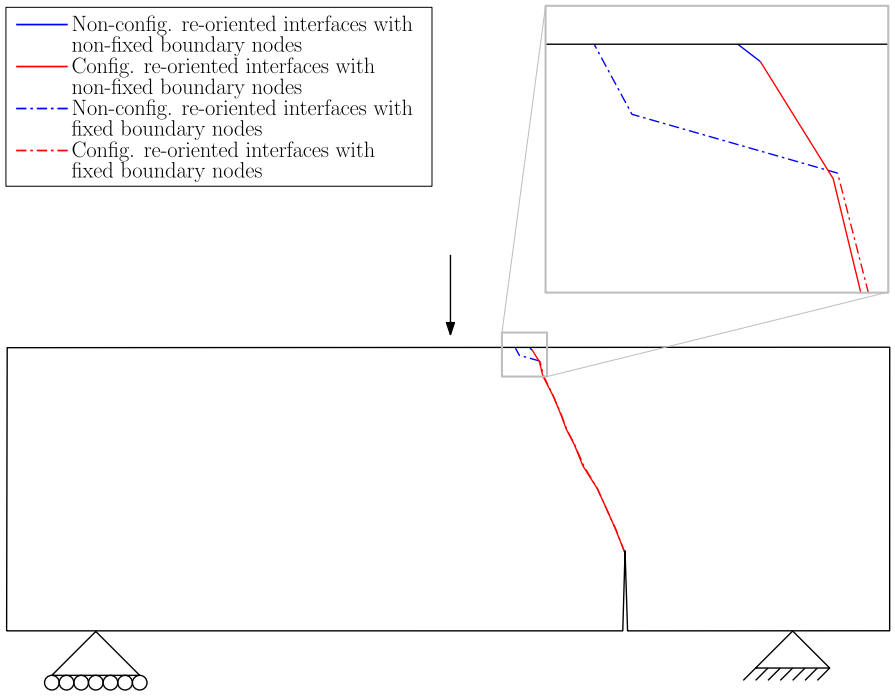

Fig. 22. Effect of moving boundary nodes w.r.t. configurationally fixed boundary nodes**.** comparison of final crack path for the eccentric three-point bending beam with $G_f^I = 0.001$ MPa·m. The dashed line represents the final trajectory with boundary nodes fixed, while the solid one is the obtained allowing the movement of boundary nodes during the mesh relaxation technique. In red, cracked interface elements that have been re-oriented by configurational forces; and in blue, un-cracked interface elements (that may have been however re-oriented by the mesh relaxation procedure). (For interpretation of the references to color in this figure legend, the reader is referred to the web version of this article.)

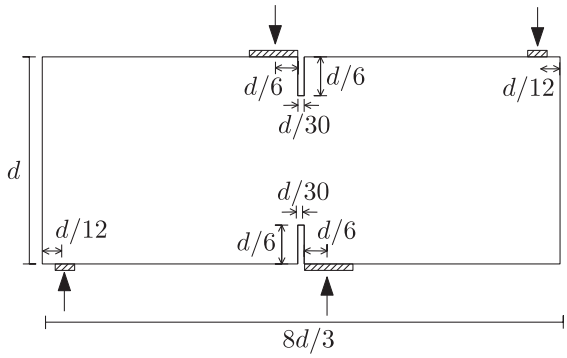

Fig. 23. Geometry and boundary conditions of a two-notch beam $d = 150$ mm.

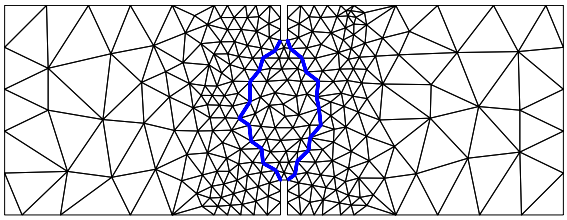

Fig. 24. Initial configuration of the two-notch beam example.

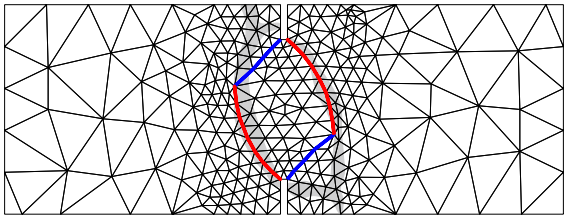

Fig. 25. Final configuration of the two-notch beam example (shaded area indicates the zones of cracking observed in experiments).

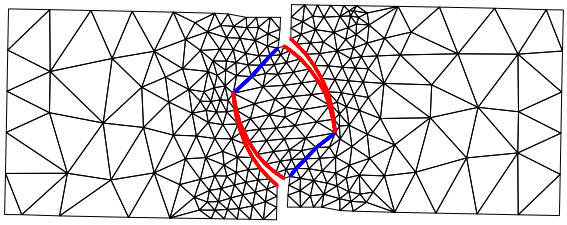

Fig. 26. Final configuration and deformation of the two-notch beam example (displacement magnification $\times 100$).

Fig. 27 depicts the mesh evolution for each individual configurational step, so that progressive mesh reorientation may be appreciated as it takes place along 13 configurational steps. At each step, the process involves the progressive relocation of the nodes that on one side belong to an opening interface element, and that at the same time are marked as configurationally free. During the iterations of a given configurational step, more than one (non-consecutive) interface elements can reach the cracking condition and be selected to change their orientation. However, it is also possible that after the iterative process one or more of those interface elements initially selected would finally remain un-cracked. In Fig. 27, these interface elements are represented in orange. On the other hand, red lines represent the interface elements that have reached their new fixed location driven by configurational forces. Finally, note that the surrounding continuum mesh (black lines) and some interface elements that have not reached cracking (in blue or orange) may also modify their position, because they may reach the configurational criterion in intermediate configurational steps (in orange), or due to the mesh relaxation technique (in blue).

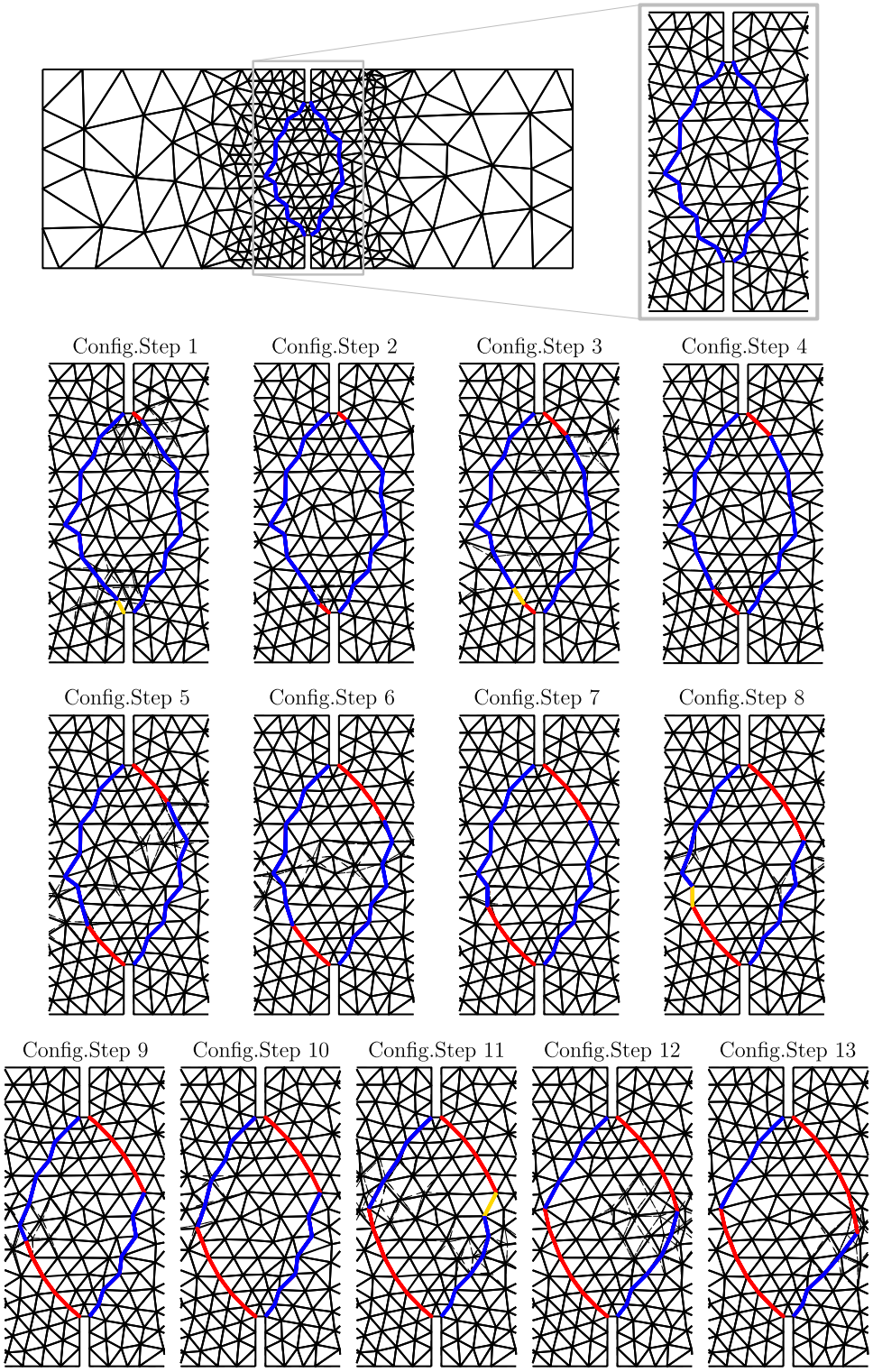

Fig. 27. Geometric evolution of the two-notch beam during configurational iterations.

5.4. Three-point bending beam with a zone of potential crack paths

The purpose of this example is to illustrate the capability of the approach developed to represent an area of possible fractures in which the potential cracks have the freedom to start, develop, compete, get arrested, etc. To this end, the case of the three-point beam bending test Section 5.1 (see Fig. 7) is considered again, with the same geometry, material parameters and boundary conditions already defined in that section. The beam is discretized again into quadratic triangular continuum elements, and the novelty is that interface elements are preinserted along all mesh lines in a central section of the beam of length dimension similar to the beam width. The resulting finite element mesh is depicted in Fig. 28, where blue lines represent the pre-inserted zero-thickness interface elements.

Fig. 29 shows the results of the calculation after prescribing a top displacement of 2.5 mm, with red lines indicating the interface elements that have been realigned during the calculation. Fig. 30 shows the same results on a deformed mesh, with a detailed view of the central part of the beam where all cracks develop.

In this example, one could think that central interface elements would develop a single fracture similar to the one obtained in the same beam example with only one crack trajectory, Section 5.1. However, Figs. 29 and 30 show various competing cracks developing near the beam center. The main one certainly is the one at the beam center as expected, but also two more have developed on each side which are progressively shorter but nevertheless comparable in length.

The obvious discussion is whether these cracks are realistic, or could be spurious secondary cracking due to the numerical strategy. In order to clarify that, a simple direct calculation has been run of the mesh of Fig. 28, that is with all the cracks (main one and secondary ones) well aligned. This has been done to the same level of prescribed displacement at the loading point, of 2.5 mm, with the results shown in Fig. 31, which depicts practically the same cracking scheme as in the configurational calculation. This example therefore confirms that at least in this case the scheme proposed is capable of representing simultaneous competing cracks within a context of systematic pre-insertion of interfaces along all mesh lines.

5.5. L-shaped panel

The last example consists of the inverted “L-shaped” panel represented in Fig. 32, which was tested experimentally in a lab campaign [77,74] and has been used as a verification test in other numerical studies, e.g. [77,78,46]. The panel is fixed along the bottom side of the inverted “L” and is subject to a vertically ascending load at the cantilever end that creates an overall bending moment. As the result, the inner side of the “L” is subject to tensile stresses, causing the panel to fail due to a dominant crack that starts at the inner vertex and progresses towards the opposite lateral face with a relatively low angle.

In the present study, the panel has been analyzed using various discretizations made with quadratic triangles for the continuum and interface elements have been pre-inserted along selected mesh lines. In the first analysis presented, interfaces are pre-inserted along all lines in a wide area along the expected crack trajectory, from the internal vertex of the structure to a point slightly higher on the right edge (Fig. 33). In order to investigate the effect of crack branching, some additional calculations have also been run with a single line of interface elements zig-zagging around the expected crack trajectory, and finally mesh sensitivity is also studied by using a refined half-mesh.

Continuum material has been assumed linear elastic (small strain) with Young’s modulus $E = 20000$ MPa and Poisson’s ratio $\nu = 0.18$. Note that this is about 20% lower than the value of E given in the original reference [77]; however, that value seemed not consistent with the elastic slope of the load-displacement curve, and it has been preferred to use a value that approaches better the experimental curve. For interface elements, the constitutive parameter values used are: normal and tangential stiffness $K_N = K_T = 10^8$MPa/m, friction angle $\tan\varphi = 0.7$, tensile strength $\chi = 2.7$ MPa, cohesion $c = 15$ MPa, sigma dilatation $\sigma_{dil} = 27$ MPa, fracture energy mode I $G_f^I = 9 \cdot 10^{-5}$ MPa·m and fracture energy mode IIa $G_f^{IIa} = 9\hat{A} \cdot 10^{-4}$ MPa·m.

In Figs. 34 and 35, the results obtained using the approach described on the basis of the mesh of Fig. 33, are shown together with the results obtained via traditional FEM+z calculation with the fixed original mesh (of the same Fig. 33). In Fig. 34, the interface elements that have started cracking are highlighted in green or red on the undeformed mesh (the undeformed original mesh in Fig. 34a, and the undeformed final mesh after configurational re-orientation in Fig. 34b), and the gray shaded area shows the scatter of the experimental results from [74,77]. Fig. 35 depicts the same results, but in this case represented on the deformed meshes. In Figs. 34b and 35b, blue lines represent the interface elements which did not reach cracking and therefore were not moved directly in the direction of configurational forces (although they might have been reoriented if they were connected to a cracked element), and red lines are the ones which have been reoriented to the optimal position. Finally, the load-displacement curves resulting from the calculation, both with the original (in blue) as well as the re-oriented mesh (in red) are represented in Fig. 39, together with the gray shaded area representing the scatter of experimental results [74,77], plus also some additional curves obtained using a single line of pre-inserted

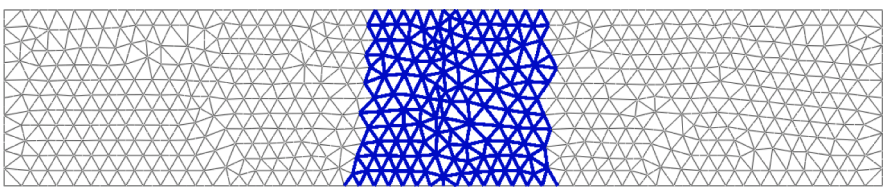

Fig. 28. Initial mesh configuration of the three-point beam bending test example.

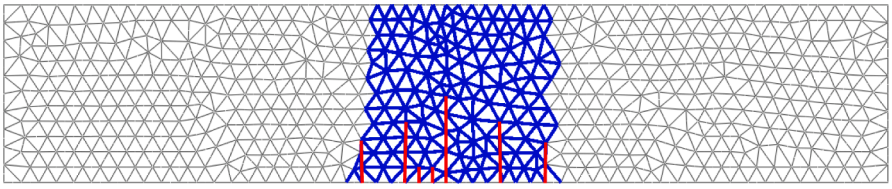

Fig. 29. Final mesh configuration of the three-point beam bending test example.

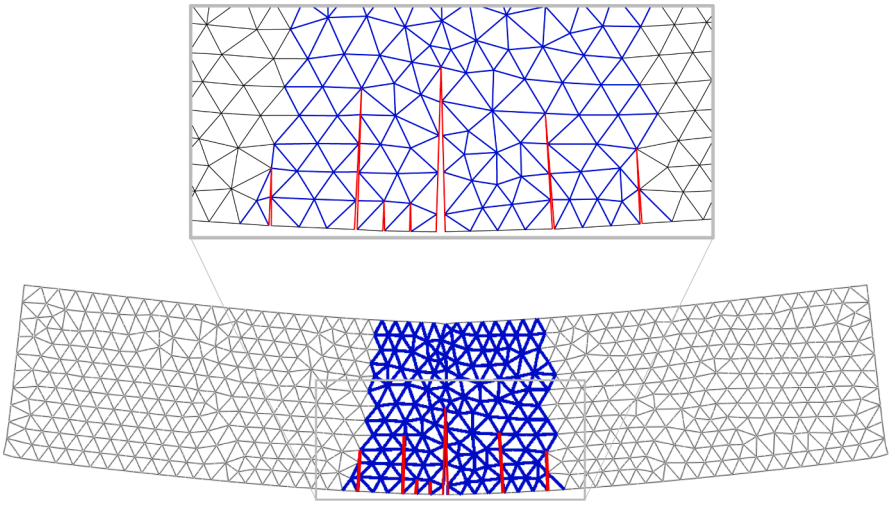

Fig. 30. Three-point bending test deformation after solving the deformational and configurational problem (displacement magnification ×100).

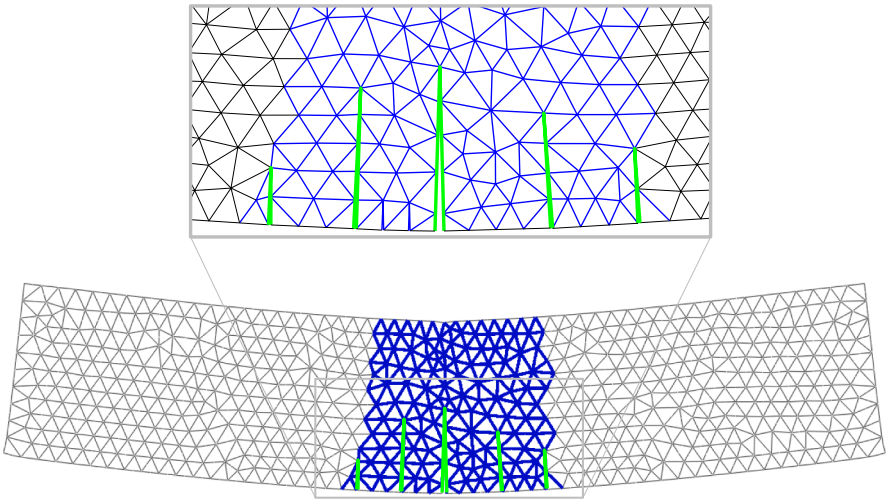

Fig. 31. Deformed mesh and cracking obtained in direct calculation using final configuration (magnification ×100).

interfaces on the same mesh and on a refined half-mesh which are described below.

As seen in the figures, the approach developed based on configurational mechanics leads in this case to results (Figs. 34a, 35a, and solid red line in Fig. 39) which fall fully within the experimental scatter, except in the tail part of load-displacement diagram, as explained below.

The results obtained with the crack realignment approach seem clearly closer to experimental behavior than the results obtained with the traditional FEM+z calculations with the fixed original mesh, which are also represented in the same figures. Indeed, those results with fixed original mesh exhibit a main crack path clearly drifting upwards, and a load-displacement curve with a substantially higher peak load and post-peak behavior than those obtained experimentally.

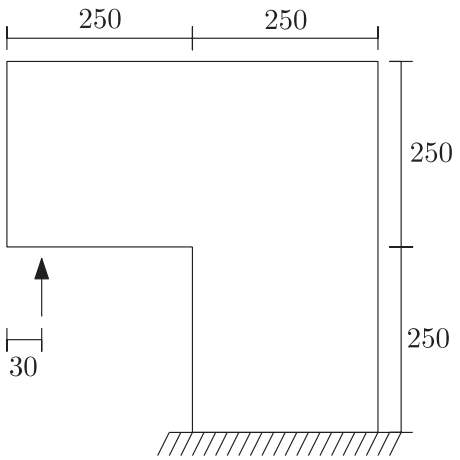

Fig. 32. Geometry and boundary conditions of the L-shaped panel.

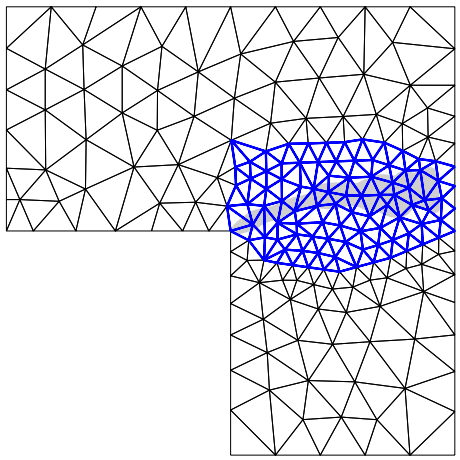

Fig. 33. Initial mesh configuration of L-Shaped panel problem. Red lines represent the zero-thickness interface elements inserted along the FEM mesh lines (in black). The expected crack path is depicted in the shaded area, which is obtained by experimental results [77]. (For interpretation of the references to color in this figure legend, the reader is referred to the web version of this article.)

The crack path obtained with the crack realignment approach also shows the occurrence of crack branching, mainly at two points: (a) a short incipient vertical branch departing upwards at about 1/4 length distance from the crack mouth, and (b) a main crack bifurcation at about 3/4 of the crack length, that divides the single crack in two competing crack symmetrically oriented about 30 degrees up and down from the axis of the main trajectory. It is worth noting that branching event (a) does not take place when the main crack reaches that point, but at a later stage, when the main crack is well developed and the upper crack wall is progressively becoming the lower side of an extension of the horizontal leg of the L-panel. Upwards cantilever bending of that panel leg causes significant tensile stresses parallel to its lower face, leading to cracking when those stresses exceed strength at the interfaces with the appropriate vertical orientation. On the other hand, the main crack branching (b) does occur when the crack tip reaches that point, due to a multiaxial tension state generated in that zone. From that point on, two competing cracks continue for the remaining part of the loading, which seems to be consistent with the widening of the final part of the shaded experimental area.

It has to be emphasized that the freedom to obtain more complex behavior than a single propagating crack, such as the above-mentioned crack branching events (a) or (b) is intrinsically “built in” in the approach proposed, as it is part of the FEM+z analysis procedure which is the basis of the current implementation. And this may be in contrast to some of the alternative existing approaches in which representing additional cracks might require additional code provisions and increased storage needs (e.g. XFEM).

In order to investigate the effect of crack branching on the crack trajectory and the load-displacement diagram, additional calculations have been run using the same original mesh as in Fig. 33, but pre-inserting interface elements only along a single line zig-zagging around the around the expected cracking zone. The analysis has been run with the approach proposed allowing mesh realignment, and also using traditional FEM+z analysis with a fixed mesh. The results in terms of final crack trajectories are represented in Fig. 36.

Also, in order to see the effect of mesh refinement, the same calculations have been run with the same single line of zig-zagging

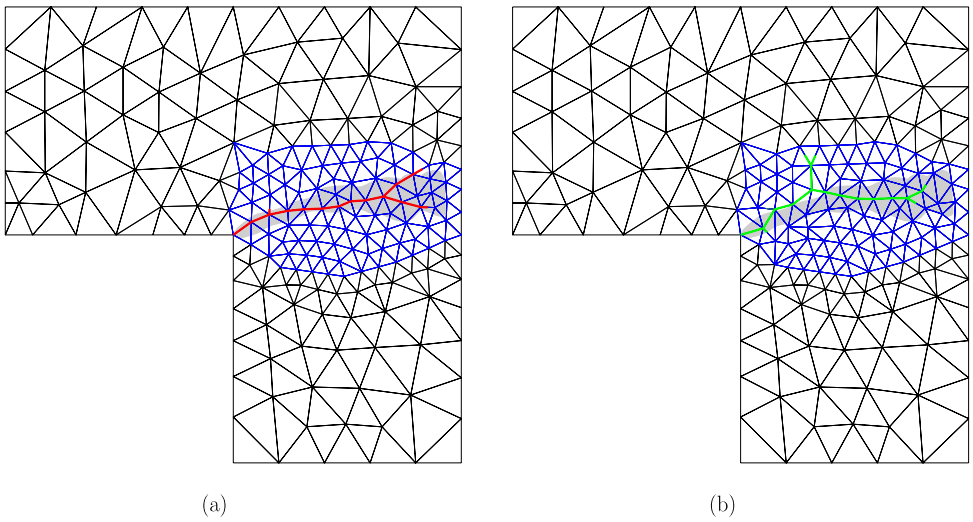

Fig. 34. L-shaped panel analysis with a zone of interface elements inserted. (a) Red lines show the main crack trajectory in the undeformed configuration at the end of the configurational procedure. (b) Green lines represent the main crack trajectory obtained in the calculation with the fixed mesh. (For interpretation of the references to color in this figure legend, the reader is referred to the web version of this article.)

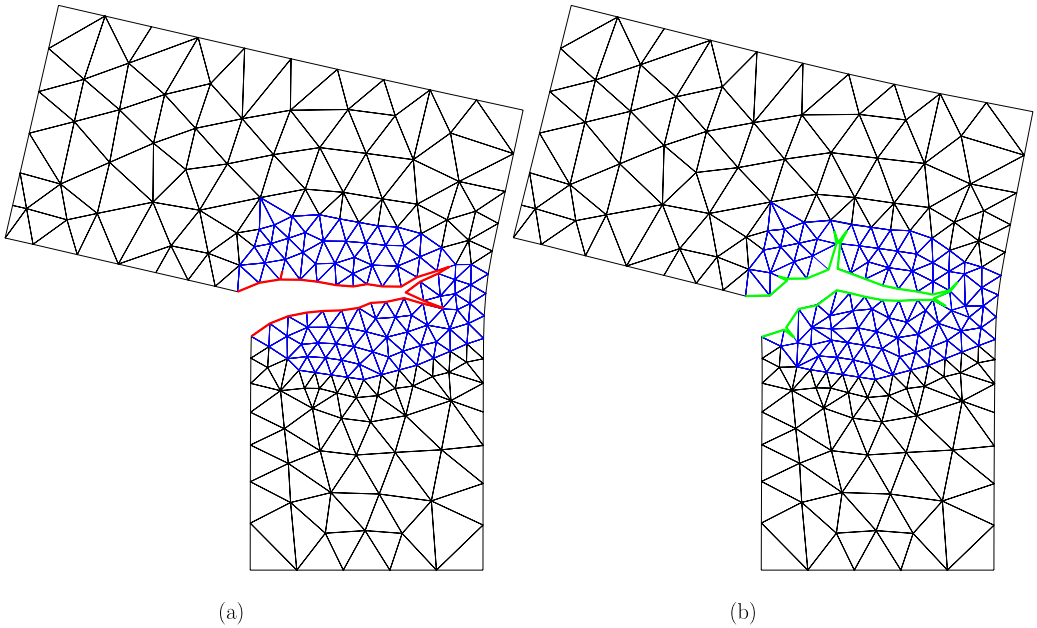

Fig. 35. Deformations and cracking of the L-Shaped panel (a) after solving the problem with the configurational procedure, and (b) after solving the problem with the fixed original mesh (displacement magnification $\times 100$).

interfaces, but a denser structured half mesh (subdividing each line in the mesh into two segments and each triangle into four smaller triangles). The results of those refined calculations in terms of final crack geometry are represented in Fig. 37. The final crack paths of all cases are represented in Fig. 38, and a comparison of all load-displacement curves is represented in Fig. 39.

The comparison of crack paths in Fig. 38, shows that the cracks obtained without mesh realignment (in green) are zig-zagging unrealistically, while those obtained with the proposed procedure for mesh re-alignment (in red) look much smoother and better aligned with the experimental shaded area. Among the calculations obtained with mesh re-alignment, the paths obtained with a single line of interfaces run straighter along the central part of the experimental scatter, and little difference is obtained with the refined mesh, for which the crack path follows a slightly lower line and more centered in the shaded area but essentially similar to the path obtained with the unrefined mesh and, for the most part, also coincident with the main path obtained in the multiple crack calculation. In the final part of the crack, approaching the right side of the panel, the single-line crack runs in between the two branches obtained for the multiple crack calculation, which seems also reasonable.

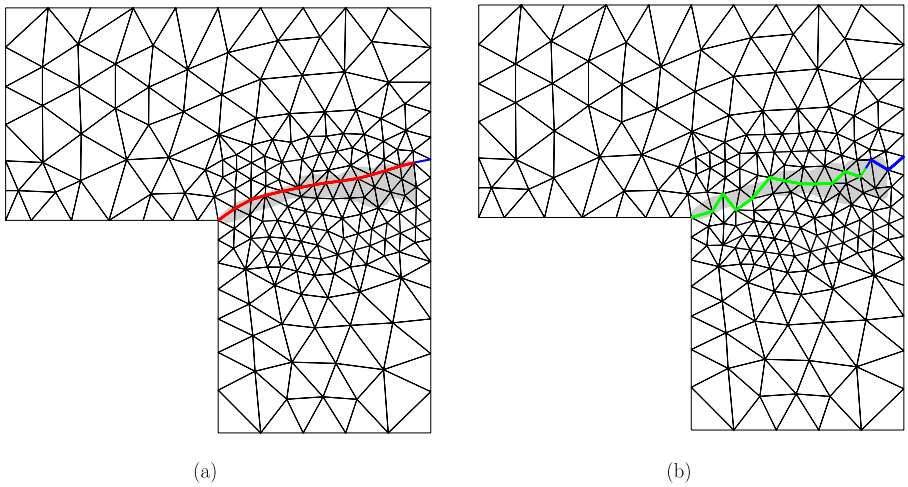

Fig. 36. L-shaped panel analysis with a single-line of interfaces inserted. (a) Red lines show the main crack trajectory obtained using the configurational procedure. (b) Green lines represent the main crack trajectory obtained in the calculation with the fixed mesh. (For interpretation of the references to color in this figure legend, the reader is referred to the web version of this article.)

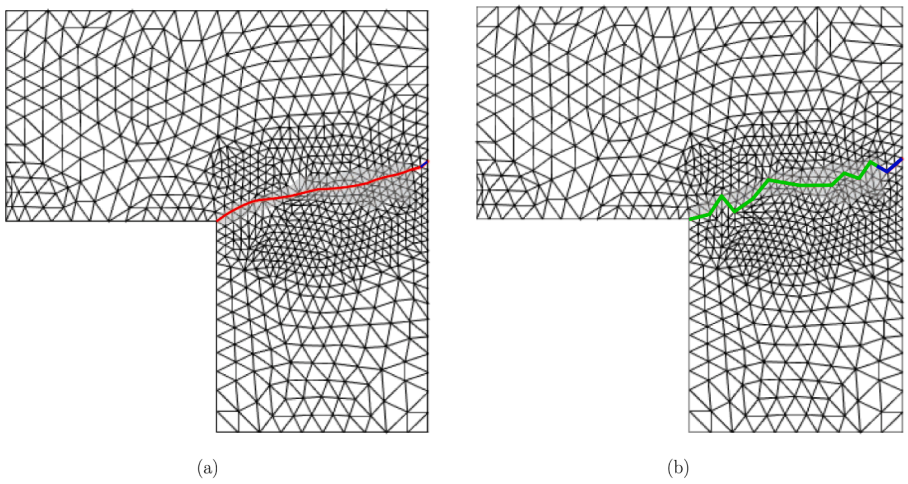

Fig. 37. L-shaped panel analysis with a single-line of interfaces inserted and structured mesh refinement. (a) Red lines show the main crack trajectory obtained using the configurational procedure. (b) Green lines represent the main crack trajectory obtained in the calculation with the fixed mesh. (For interpretation of the references to color in this figure legend, the reader is referred to the web version of this article.)

The comparison of load-displacement curves in Fig. 39, also shows that the re-alignment strategy based on configurational mechanics leads to load-displacement curves that are much closer to experimental behavior than those obtained without crack re-alignment, which show much higher (and in some curves unrealistically higher) peak and post-peak responses. Also, little difference is observed between curve for the refined and unrefined single-line crack, both for the fixed mesh and the re-aligned mesh calculations.

Among the load-displacement curves obtained with interface re-alignment, the curve for multiple cracking runs always above the curves obtained with a single interface line, which may be explained because of the higher energy dissipation implied by crack branching. It is also observed that in the tail part of the diagram, the difference between curves is progressively amplified; the curve for multiple cracking drifts progressively out of the shaded experimental area on its upper limit, while the curves obtained with a single line of interfaces run on its lower limit. This seems also consistent with the progressively higher difference in dissipation caused by the difference in the total crack length, minimal in case of a single crack, and probably an upper bound in the case of two equally competing cracks as obtained in the analysis with multiple cracking allowed.

6. Concluding remarks

A numerical approach has been presented to evaluate the crack propagation along non-preestablished paths by combining

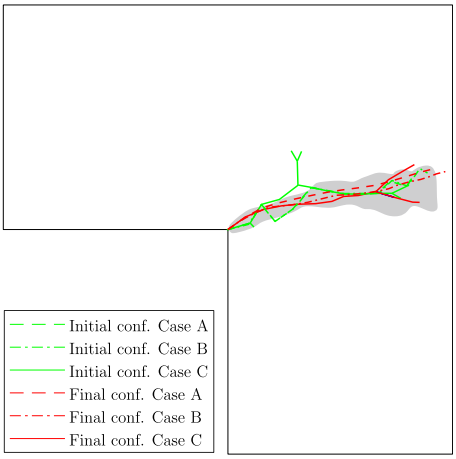

Fig. 38. Comparison of crack paths obtained for the L-shaped panel analysis**.** In red paths obtained using interface re-alignment approach, and in green fixed original mesh with**.** (A) single line of interfaces, (B) single line of interfaces and structured half-mesh refinement, and (C) interfaces along all mesh lines in the zone of potential cracking. (For interpretation of the references to color in this figure legend, the reader is referred to the web version of this article.)

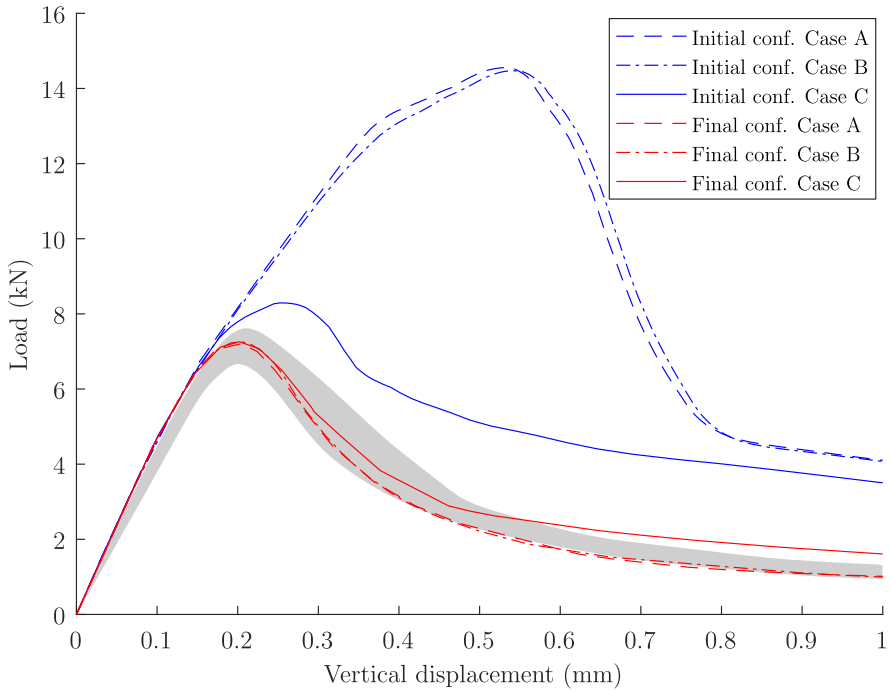

Fig. 39. Load-displacement curves of L-shaped panel problem obtained with analysis with the original mesh fixed, and allowing configurational realignment process.

traditional zero-thickness interface elements (FEM+z) with a mesh re-alignment strategy based on concepts of configurational mechanics.

The approach is conceptually simple but the success of its practical implementation depends very much on the details of the various non-trivial procedures involved. Relocating nodes according to the directions of configurational forces may become very complicated and potentially unmanageable when too many nodes are moved at the same time. Configurationally prescribed nodes have to be defined to avoid changing some fundamental parameters such as domain geometry or dimensions. Also, the procedure may get polluted by "configurational noise" coming from the oscillation of total energy with nodal positions, which is inevitably associated to the intrinsic FE discretization error. For those reasons, a selective methodology of node configurational release has been developed to move only the crack tip nodes when the corresponding interface starts to open, and this is accompanied by a mesh relaxation procedure

to preserve mesh quality in surrounding elements after each crack tip relocation.

Another crucial point is from what earlier point in the loading history the analysis has to be restarted after each mesh re-alignment operation, since it is obvious that, with a better aligned interface, cracking may be starting at a lower load level. In the present implementation, the analysis is restarted from the last configurationally converged step. In the examples analyzed this has led to consistent results which have been verified by straight analysis with a standard FEM+z analysis using final crack configuration as a fixed mesh. However, this aspect remains the subject of further research.

The first application examples include cases for which the final fracture trajectory is known, either by symmetry considerations or by experimental results. Three-point bending examples show that, in spite of different initial mesh configurations, the dominant fracture ends up being totally vertical and aligned with the imposed load or displacement. The examples of eccentric three-point bending test, L-shaped panel and mixed mode fracture tests develop more complex trajectories that compare well with experimental tests. In most cases, the resulting crack trajectory and overall load-displacement curves are compared advantageously with those obtained using traditional FEM+z analysis on the fixed initial mesh. Additional aspects that have been explored in examples are moving boundary nodes in the relaxation process, and influence of mesh refinement.

The main advantages of the proposed method are: (1) it incorporates the very fundamental assumption that fractures propagate in the direction of maximum structural energy release (global criterion and not local); and (2) the correct energy dissipation due to fracture propagation is ensured by the underlying FEM+z (zero-thickness interface) approach that is actually running on the mesh once it has been properly realigned.

In conclusion, the approach developed seems to represent an advantageous promising strategy for crack propagation which is conceptually simpler and computationally cheaper than other alternative procedures requiring either much denser meshes in fracture zones of a-priori unknown location, or other external artifacts such as non-mechanics tracking algorithms.

Declaration of Competing Interest

The authors declare that they have no known competing financial interests or personal relationships that could have appeared to influence the work reported in this paper.

Acknowledgements

The work has been partially supported by research grants BIA2016-76543-R from MEC (Madrid), which includes FEDER funds from the European Union, and 2017SGR-1153 from Generalitat de Catalunya (Barcelona). The first author would also like to thank MICINN (Madrid) for the FPI doctoral fellowship received.

References

[1] Wu T, Carpiuc-Prisacari A, Poncelet M, de Lorenzis L. Phase-field simulation of interactive mixed-mode fracture tests on cement mortar with full-field displacement boundary conditions. Eng Fract Mech 2017.
[2] Steinmann P, Scherer M, Denzer R. Secret and joy of configurational mechanics: From foundations in continuum mechanics to applications in computational mechanics. ZAMM J Appl Math Mech 2009;89:614–30.
[3] Kaczmarczyk Ł, Ullah Z, Pearce CJ. Energy consistent framework for continuously evolving 3D crack propagation. Comput Methods Appl Mech Eng 2017;324:54–73.
[4] Patil RU, Mishra BK, Singh IV. An adaptive multiscale phase field method for brittle fracture. Comput Methods Appl Mech Eng 2018;329:254–88.
[5] Lu G, Chen J. A new nonlocal macro-meso-scale consistent damage model for crack modeling of quasi-brittle materials. Comput Methods Appl Mech Eng 2020;362:112802.
[6] Rashid YR. Ultimate strength analysis of prestressed concrete pressure vessels. Nucl Eng Des 1968;7:334–44.
[7] Rots JG. Computational modeling of concrete fracture. Ph.D. thesis. Technische Universiteit Delft; 1988.
[8] Bazant ZP, Oh BH. Crack band theory for fracture of concrete. Matériaux et construction 1983;16:155–77.
[9] Pijaudier-Cabot G, Bazant ZP. Nonlocal damage theory. ASCE J Eng Mech 1987;113:1512–33.
[10] Lasry D, Belytschko T. Localization limiters in transient problems. Int J Solids Struct 1988;24:581–97.
[11] de Borst R, Pamin J, Peerlings R, Sluys L. On gradient-enhanced damage and plasticity models for failure in quasi-brittle and frictional materials. Comput Mech 1995;17:130–41.
[12] Peerlings RH. Enhanced damage modelling for fracture and fatigue [Ph.D. thesis]. Eindhoven (The Netherlands): Technische Universiteit Eindhoven; 1999.
[13] de Borst R. Fracture in quasi-brittle materials: a review of continuum damaged-based approaches. Eng Fract Mech 2002;69:95–112.
[14] de Borst R, Remmers J, Needleman A, Abellan M. Discrete vs smeared crack models for concrete fracture: bridging the gap. Int J Numer Anal Meth Geomech 2004;28:583–607.
[15] Miehe C, Hofacker M, Welschinger F. A phase field model for rate-independent crack propagation: Robust algorithmic implementation based on operator splits. Comput Methods Appl Mech Eng 2010;199:2765–78.
[16] Wu T, de Lorenzis L. A phase-field approach to fracture coupled with diffusion. Comput Methods Appl Mech Eng 2016;312:196–223.
[17] Miehe C, Welschinger F, Hofacker M. Thermodynamically consistent phase-field models of fracture: Variational principles and multi-field FE implementations. Int J Numer Meth Eng 2010;83:1273–311.
[18] Takezawa A, Nishiwaki S, Kitamura M. Shape and topology optimization based on the phase field method and sensitivity analysis. J Comput Phys 2010;229:2697–718.
[19] Giovanardi B, Scotti A, Formaggia L. A hybrid XFEM-Phase field (Xfield) method for crack propagation in brittle elastic materials. Comput Methods Appl Mech Eng 2017;320:396–420.
[20] Ngo D, Scordelis AC. Finite element analysis of reinforced concrete beams. J Proc 1967;64:152–63.
[21] Ingraffea AR, Linsbauer HN, Rossmanith HP. Computer simulation of cracking in a large arch dam: downstream side cracking. Fracture of Concrete and Rock, Verlag, NY (USA) 1987:334–42.
[22] Hillerborg K, Modéer M, Petersson P. Analysis of crack formation and crack growth in concrete by means of fracture mechanics and finite elements. Cem Concr Res 1976;6:773–81.
[23] Stankowski T, Runesson K, Sture S. Fracture and slip of interfaces in cementitious composites. I: characteristics. J Eng Mech 1993;2:292–314.

[24] Carol I, Prat P, López CM. Normal/shear cracking model: application to discrete crack analysis. J Eng Mech 1997;123:765–73.
[25] Caballero A, William KJ, Carol I. Consistent tangent formulation for 3D interface modeling of cracking/fracture in quasi-brittle materials. Comput Methods Appl Mech Eng 2008;197:2804–22.
[26] Wu T, Wriggers P. Multiscale diffusion-thermal–mechanical cohesive zone model for concrete. Comput Mech 2015;66:999–1016.
[27] Stankowski T. Numerical simulation of progressive failure in particle composites. Ph.D. thesis. Boulder (USA): University of Colorado; 1990.
[28] Vonk RA. Softening of concrete loaded in compression. Ph.D. thesis. Eindhoven (The Netherlands): Eindhoven University of Technology; 1992.
[29] Carol I, López CM. Fracture-based interface model: theory, implementation and aplications. In: Idelsohn S, Oñate E, Dvorkin E., editors. Computational Mechanics. Barcelona: CIMNE; 1998.
[30] López CM. Análisis microestructural de la fractura del hormigón utilizando elementos finitos tipo junta. Aplicación a diferentes hormigones. Ph.D. thesis. Barcelona, Barcelona: Universitat Polit'ecnica de Catalunya (UPC); 1999.
[31] Camacho GT, Ortiz M. Computational modelling of impact damage in brittle materials. Int J Solids Struct 1996;33:2899–938.
[32] Dvorkin EN, Cuitiño AM, Gioia G. Finite elements with displacement interpolated embedded localization lines insensitive to mesh size and distortions. Int J Numer Meth Eng 1990;30:541–64.
[33] Belytschko T, Krongauz Y, Organ D, Fleming M, Krysl P. Meshless methods: an overview and recent developments. Comput Methods Appl Mech Eng 1996;139:3–47.
[34] Belytschko T, Black T. Elastic crack growth in finite elements with minimal remeshing. Int J Numer Meth Eng 1999;45:601–20.
[35] Wells GN, Sluys LJ. Three-dimensional embedded discontinuity model for brittle fracture. Int J Solids Struct 2001;38:897–913.
[36] Zi G, Belytschko T. New crack-tip elements for XFEM and applications to cohesive cracks. Int J Numer Meth Eng 2003;57:2221–40.
[37] Borja RI. Assumed enhanced strain and the extended finite element methods: A unification of concepts. Comput Methods Appl Mech Eng 2008;197:2789–803.
[38] Nguyen VP, Rabczuk T, Bordas S, Duflot M. Meshless methods: a review and computer implementation aspects. Math Comput Simul 2008;79:763–813.
[39] Belytschko T, Gracie R, Ventura G. A review of extended/generalized finite element methods for material modeling. Modell Simul Mater Sci Eng 2009;17.
[40] Das KC, Ausas RF, Segura JM, Narang A, Rodrigues ER, Carol I, et al. Efem vs. XFEM: a comparative study for modeling strong discontinuity in geomechanics. In: 13th ISRM International Congress of Rock Mechanics. International Society for Rock Mechanics and Rock Engineering.
[41] Möes N, Dolbow J, Belytschko T. A finite element method for crack growth without remeshing. Int J Numer Methods Eng 1999:131–50.
[42] Das KC, Sandha SS, Carol I, Vargas PE, González NA, Rodrigues E, et al. Multiple intersecting cohesive discontinuities in 3D reservoir Geomechanics. In: Proc. 50th US Rock Mechanics/Geomechanics Symposium. Houston, TX (USA): American Rock Mechanics Association (ARMA).
[43] Crusat L, Carol I, Garolera D. XFEM formulation with sub-interpolation, and equivalence to zero-thickness interface elements. Int J Numer Anal Meth Geomech 2019;43:45–76.
[44] Jirásek M. Comparative study on finite elements with embedded discontinuities. Comput Methods Appl Mech Eng 2000;188:307–30.
[45] Unger JF, Eckardt S, Könke C. Modelling of cohesive crack growth in concrete structures with the extended finite element method. Comput Methods Appl Mech Eng 2007;196:4087–100.
[46] Meschke G, Dumstorff P. Energy-based modeling of cohesive and cohesionless cracks via X-FEM. Comput Methods Appl Mech Eng 2007;196:2338–57.
[47] Chahine E, Laborde P, Renard Y. Crack tip enrichment in the XFEM using a cutoff function. Int J Numer Meth Eng 2008;75:629–46.
[48] Chevaugeon N, Moës N, Minnebo H. Improved crack tip enrichment functions and integration for crack modeling using the extended finite element method. Int J Multiscale Comput Eng 2013;11.
[49] Watanabe N, Wang W, Taron J, Görke U, Kolditz O. Lower-dimensional interface elements with local enrichment: application to coupled hydro-mechanical problems in discretely fractured porous media. Int J Numer Meth Eng 2012;90:1010–34.
[50] Zi G, Song JH, Budyn E, Lee SH, Belytschko T. A method for growing multiple cracks without remeshing and its application to fatigue crack growth. Modell Simul Mater Sci Eng 2004;12:901.
[51] Lang C, Makhija D, Doostan A, Maute K. A simple and efficient preconditioning scheme for heaviside enriched XFEM. Comput Mech 2014;54:1357–74.
[52] Fries TP, Belytschko T. The extended/generalized finite element method: an overview of the method and its applications. Int J Numer Meth Eng 2010;84:253–304.
[53] Erdogan F, Sih GC. On the crack extension in plates under plane loading and transverse shear. J Basic Eng 1963;85:519–25.
[54] Nuismer RJ. An energy release rate criterion for mixed mode fracture. Int J Fract 1975;11:245–50.
[55] Yang Z, Chen J. Fully automatic modelling of cohesive discrete crack propagation in concrete beams using local arc-length methods. Int J Solids Struct 2004;41:801–26.
[56] Dumstorff P, Meschke G. Crack propagation criteria in the framework of X-FEM based structural analyses. Int J Numer Anal Meth Geomech 2007;31:239–59.
[57] Eshelby JD. The elastic energy-momentum tensor. J Elast 1975;5:321–35.
[58] Denzer R, Barth FJ, Steinmann P. Studies in elastic fracture mechanics based on the material force method. Int J Numer Meth Eng 2003;58:1817–35.
[59] Nguyen TD, Govindjee S, Klein PA, Gao H. A material force method for inelastic fracture mechanics. J Mech Phys Solids 2005;53:91–121.
[60] Steinmann P, Maugin GA, editors. Mechanics of material forces. Springer-Verlag; 2005.
[61] Miehe C, Gürses E, Birkle M. A computational framework of configurational-force-driven brittle fracture based on incremental energy minimization. In: Int J Fract, 145; 2007. p. 245–9.
[62] Kaczmarczyk Ł., Nezhad MM, Pearce C. Three-dimensional brittle fracture: configurational-force-driven crack propagation. Int J Numer Methods Eng 2014;97:531–50.
[63] Crusat L. Numerical modeling of cracking along non-preestablished paths. Ph.D. thesis. Barcelona: Universitat Politècnica de Catalunya (UPC); 2019.
[64] Crusat L, Carol I. Configurational forces in fea: local coordinate derivative, and discretization error vs. physical effect [submitted for publication].
[65] Mueller R, Maugin GA. On material forces and finite element discretizations. Comput Mech 2002;29:52–60.
[66] Goodman RE, Taylor RL, Brekke TL. A model for the mechanics of jointed rock. J Soil Mech Found Div 1968;94:637–59.
[67] Zienkiewicz OC, Best B, Dullage C, Stagg KG. Analysis of nonlinear problems in rock mechanics with particular reference to jointed rock systems. Proceedings of the Second International Congress on Rock Mechanics. 1970.
[68] Gens A, Carol I, Alonso EE. An interface element formulation for the analysis of soil-reinforcement interaction. Comput Geotech 1989;7:133–51.
[69] Crusat L, Carol I. On IDC methods based on constitutive dissipation: model-independent implementation, and combination with cylindrical Arc-Length [submitted for publication].
[70] Mueller R, Kolling S, Gross D. On configurational forces in the context of the finite element method. Int J Numer Meth Eng 2002.
[71] Frey WH, Field DA. Mesh relaxation: a new technique for improving triangulations. Int J Numer Meth Eng 1991;31:1121–33.
[72] Schweingruber M, Rank E. Adaptive mesh generation for triangular or quadrilateral elements. Proceedings of the First European Conference on Numerical Methods, Brussels, Belgium. 1992.
[73] García VO. Estudio de la fractura en modo mixto de los materiales cuasifrágiles: aplicación al hormigón convencional y al hormigón de alta resistencia. Ph.D. thesis. Barcelona: Universitat Politècnica de Catalunya (UPC); 1997.
[74] Feist C, Kerber W, Lehar H, Hofstetter G. A comparative study of numerical models for concrete cracking. European Congress on Computational Methods in Applied Sciences and Engineering (ECCOMAS). 2004.
[75] Nooru-Mohamed MB. Mixed-mode fracture of concrete: An experimental approach. Ph.D. thesis. Delft (The Netherlands): Delft University of Technology; 1992.
[76] Zhu WC, Tang CA. Numerical simulation on shear fracture process of concrete using mesoscopic mechanical model. Constr Build Mater 2002;16:453–63.
[77] Winkler B. Traglastuntersuchungen von unbewehrten und bewehrten Betonstrukturen auf der Grundlage eines objektiven Werkstoffgesetzes für Beton. Ph.D. thesis. Innsbruck (Austria): University of Innsbruck; 2001.
[78] Ambati M, Gerasimov T, De Lorenzis L. A review on phase-field models of brittle fracture and a new fast hybrid formulation. Comput Mech 2015;55:383–405.

Glossary

$\widehat{\mathbf{B}}$: non-symmetric version of the traditional "**B**" matrix in the FEM
c: cohesion
E: elastic or Young's modulus
F: cracking surface function
$\boldsymbol{F}$: deformation gradient
$\widehat{\mathbf{f}}$: configurational force
$\widehat{\mathbf{f}}^{a}$: configurational force evaluated in cluster "a"
$\widehat{\mathbf{f}}_{N}^{a}$: normal projection of configurational force evaluated in cluster "a"
G_f^I: fracture energy in Mode I
G_f^{IIa}: fracture energy in Mode IIa
$\boldsymbol{I}$: identity matrix
$iincr$: deformational increment "i"
K_N: normal stiffness coefficient
K_T: tangential stiffness coefficient
$\boldsymbol{P}$: first Piola-Kirchoff stress
w: elastic energy per integration point
W: elastic energy per unit volume of the undeformed configuration
W_{cr}: Work Spent on Fracture Processes
W_{el}: elastic energy of a continuum finite element
$\boldsymbol{x}$: nodal coordinates in the current configuration
$\boldsymbol{X}$: nodal coordinates in the reference configuration
$\boldsymbol{X}_{new}$: new nodal coordinates
$\boldsymbol{X}_{old}$: previous nodal coordinates
α: small constant value
$\widehat{\alpha}$: trigonometrical function that returns an scalar deppending on $\Delta\theta$ value
χ: tensile strength
$\Delta\theta$: angle incrementation
ε: strain tensor
ν: Poisson's ratio. σ stress tensor
$\widehat{\sigma}$: small-strain configurational stress
σ_N: interface normal stress
σ_T: interface tangential stress
σ_{dil}: limit stress dilatancy
$\boldsymbol{\Sigma}$: large-strain configurational stress tensor or Eshelby's energy-momentum tensor. φ tangent of internal friction angle
ψ: global energy of the system
CM: Configurational Mechanics
EFEM: Embedded Finite Element Method
FCM: Fictitious Crack Model
FEM: Finite Element Method
FEM+z: Finite Element Method with zero-thickness interface elements pre-inserted between continuum elements
FM: Fracture Mechanics
IDC: Indirect Displacement Control
LEFM: Linear Elastic Fracture Mechanics
XFEM: eXtended Finite Element Method